

The selection of the data for calculating the amounts of evaporation at the various sites and the method of calculation are described in the following section.

### 6.3.2 Calculation of Evaporation from Reservoir Surface

#### (1) Goktas Reservoir

##### (a) Air Temperature

Air temperature observation data on the vicinity of the Goktas project site are available from the Feke Meteorological Station in operation since September 1965. Since the elevation of Goktas Reservoir (high water level: 630 m) would be approximately the same as the elevation, 620 m, of Feke Meteorological Station, it was decided to use the air temperatures at the Feke Station directly as air temperatures at the Goktas Reservoir. However, the air temperature observation data of Feke Meteorological Station are available since September 1965. Therefore, for the period before August 1965, the air temperatures at the Feke Station are calculated by the following equation with the air temperature data of the Adana station, located in the Mediterranean region to which the Goktas site belongs, and having a good correlation of monthly mean air temperatures with that of the Feke Station shown in Fig. 6-19 (correlation coefficient 0.992):

$$TFK = 1.19 * TAD - 7.46$$

where, TFK: monthly mean air temperature at the Feke Station  
(°C)

TAD: monthly mean air temperature at the Adana Station  
(°C)

However, since measurements of air temperatures at the Adana Station were missing for the two years of 1948 and 1967, the correlation between the monthly mean air temperatures of the Feke Station and the Kayseri Station (correlation coefficient 0.979) is used and the air temperatures at the Feke Station are supplemented by the following equation:

$$TFK = 0.91 * TKY + 6.19$$

where, TKY: monthly mean air temperature at the Kayseri Station (°C)

The air temperatures at the Feke Station obtained in such manner are used as the air temperatures at the Goktas reservoir site. The results of calculations are given in Table 6-21.

(b) Evaporation

With regard to measurement data of evaporation in the vicinity of the Goktas project site there are the data of the Musahacili Meteorological Station. However, this site belongs to the Central Anatolian Region and the climatic characteristics are different from those of the Goktas project site. Furthermore, air temperatures have not been observed at the Musahacili Station so that the relationship between amount of evaporation and air temperature is not known. Therefore, the correlations of air temperatures at the Feke site were investigated for the Goksun and Adana Station which are located in the Mediterranean climate region. As a result, it is decided to use the air temperatures and amounts of evaporation at the Adana Station having the better correlation with the air temperature at the Feke Station (correlation coefficient 0.992).

The relationship between monthly evaporation and monthly mean air temperature at the Adana Station is shown in Fig. 6-20. This relationship is applied to the Goktas reservoir site and the evaporation from Goktas Reservoir is calculated by the following equation:

$$EGO = (10.02 * TGO - 62.31) * 0.7$$

where, EGO: monthly evaporation from the surface of the Goktas Reservoir (mm)

TGO: monthly mean air temperature at the Goktas Reservoir Site (°C)

Fig. 6-19 Correlation between the Monthly Mean Temperature Values of Adana and Feké Meteorological Stations

R= 0.992      COUNT= 244      6509 -      8612

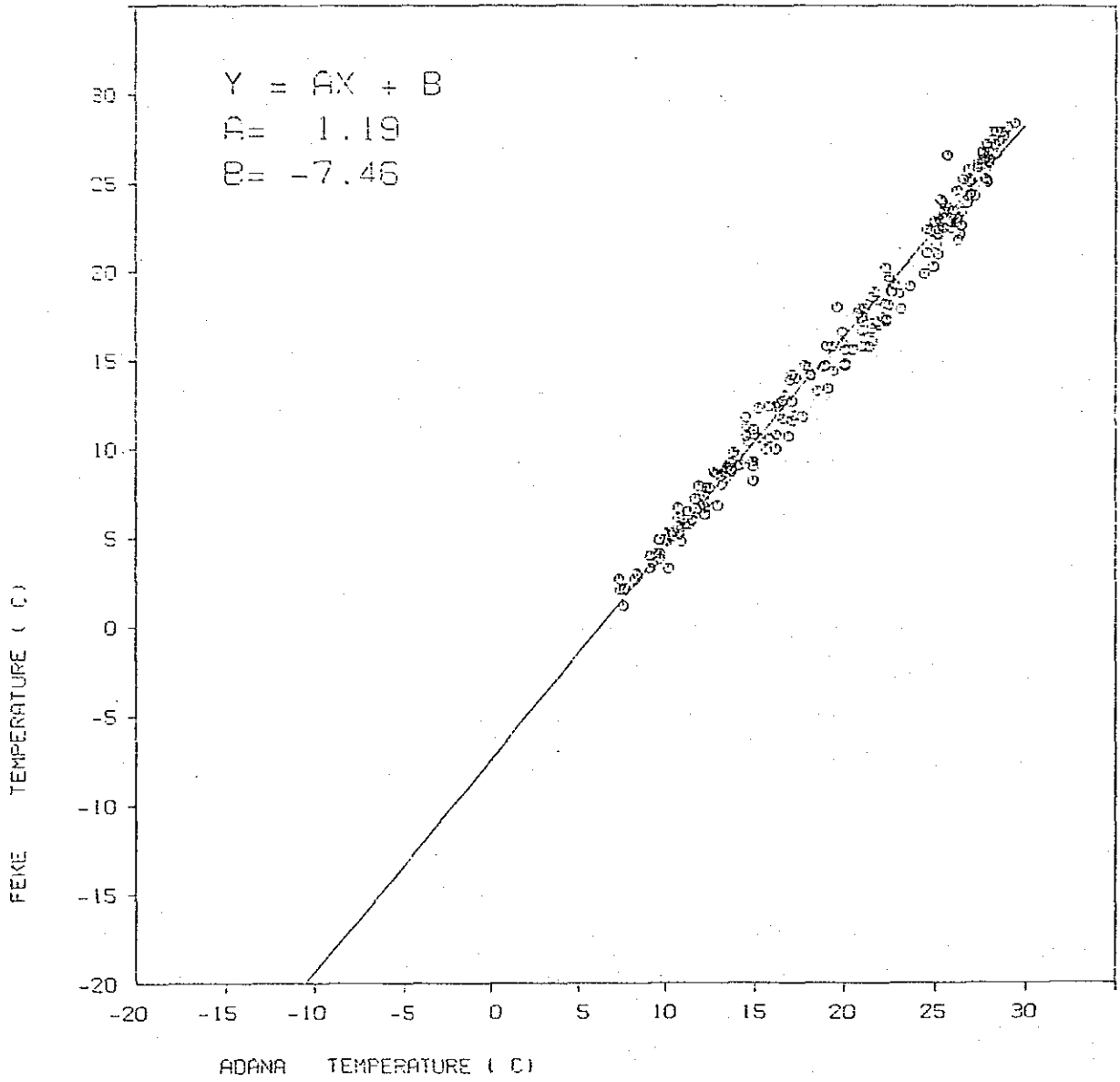
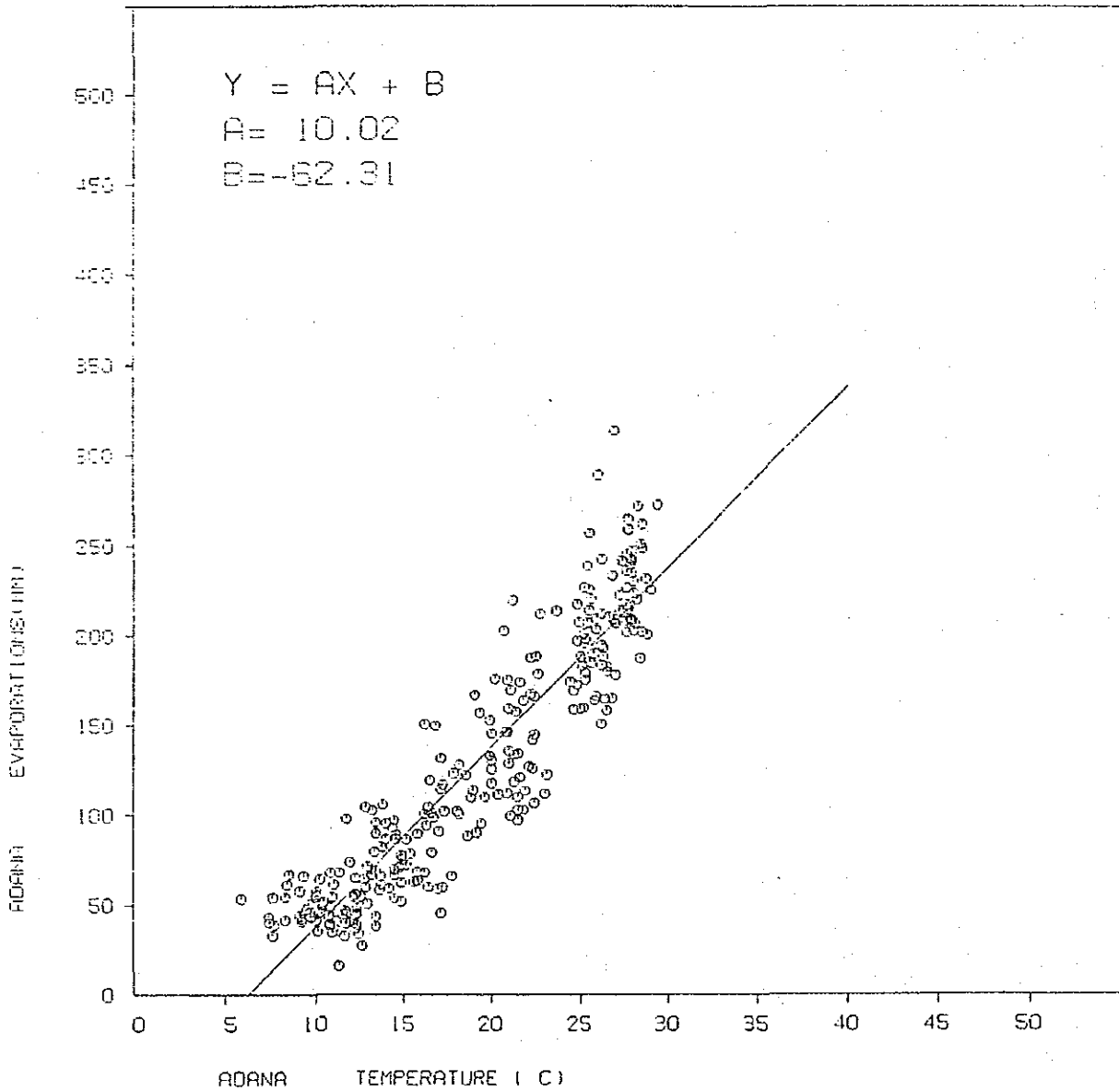


Table 6-21 Supplemented Monthly Mean Temperatures at the Feke Station (unit: °C)

YEAR	JAN	FEB	MAR	APR	MAY	JUN	JUL	AUG	SEP	OCT	NOV	DEC	MEAN
1940	3.3	6.0	7.1	13.6	16.3	22.2	24.7	25.1	21.8	17.5	11.0	6.7	14.6
1941	4.1	7.1	7.9	13.0	19.9	22.8	25.3	25.6	21.6	14.2	10.0	1.5	14.5
1942	0.5	6.2	8.2	12.4	18.4	24.0	25.3	25.1	21.9	16.7	10.6	5.0	14.6
1943	2.9	2.5	4.4	10.3	16.3	20.6	24.2	26.6	20.6	19.0	13.4	6.7	14.3
1944	2.7	4.8	8.8	13.5	16.5	22.1	24.9	24.9	21.9	17.8	10.7	6.1	14.6
1945	3.4	4.0	5.2	10.6	20.3	22.4	25.9	26.2	23.6	16.3	11.2	5.0	14.6
1946	3.8	4.2	7.4	13.4	16.8	22.4	25.6	26.5	24.4	15.2	13.8	6.7	15.1
1947	4.2	5.6	10.9	14.1	19.1	22.6	26.2	26.3	22.1	16.9	12.1	7.1	15.7
1948	8.6	8.2	6.5	14.6	19.8	23.9	26.8	27.1	21.5	15.4	7.7	3.2	15.3
1949	2.2	1.2	6.6	9.4	18.6	21.7	23.8	24.7	19.4	16.5	13.0	6.1	13.7
1950	-1.0	1.9	7.9	15.5	16.9	21.6	24.7	24.7	23.0	15.3	11.2	7.3	14.1
1951	4.3	5.5	10.2	13.7	17.8	22.2	25.3	26.1	22.6	14.4	10.7	4.0	14.0
1952	4.0	5.5	6.3	12.8	16.9	21.9	24.9	26.2	24.9	18.7	10.5	8.4	15.1
1953	4.4	4.8	4.1	11.8	16.7	22.2	26.0	26.1	21.1	16.7	7.2	1.2	13.6
1954	1.7	4.8	9.7	10.9	16.9	23.2	26.7	27.2	22.9	17.9	11.5	6.5	15.1
1955	5.4	8.1	8.0	12.5	18.2	24.2	25.6	24.7	22.8	19.3	11.6	6.3	15.6
1956	4.3	5.7	6.2	12.7	16.1	23.0	26.1	27.1	22.3	15.9	10.2	3.8	14.5
1957	2.5	6.1	9.3	13.0	17.1	23.7	26.0	26.7	23.2	19.7	10.7	5.4	15.3
1958	4.2	6.2	9.2	12.8	17.5	21.8	24.6	26.5	21.8	16.5	11.8	6.7	15.0
1959	5.6	-0.2	7.9	13.8	18.4	21.3	24.4	25.1	20.7	14.8	10.3	6.9	14.2
1960	5.4	6.1	8.4	13.2	20.1	22.4	25.6	25.9	22.9	19.0	13.5	9.0	16.0
1961	4.0	3.7	7.3	13.0	18.4	22.0	26.1	26.6	20.5	16.6	10.9	7.2	14.9
1962	5.6	4.4	11.1	12.3	18.6	22.9	25.4	27.1	23.7	17.9	14.7	7.5	16.0
1963	6.9	7.8	6.5	13.0	16.3	22.1	25.4	26.5	23.2	18.2	11.3	5.4	15.3
1964	-0.4	4.6	9.9	12.5	16.6	22.1	25.0	25.5	25.4	18.0	10.9	6.5	14.7
1965	4.4	4.4	9.7	12.2	17.4	23.7	25.5	25.6	26.6	13.3	8.2	6.6	14.9
1966	6.7	9.2	9.8	14.2	18.2	23.5	26.8	27.4	22.2	17.3	13.4	7.2	16.4
1967	2.7	1.0	8.1	14.0	19.3	21.5	24.8	24.8	22.9	16.5	9.6	7.2	14.3
1968	2.1	4.9	8.6	15.8	19.2	22.6	27.2	24.3	19.9	15.8	10.6	6.7	14.8
1969	4.9	6.0	10.4	10.8	19.3	23.5	25.8	26.8	23.0	16.7	9.3	6.9	15.3
1970	6.5	7.6	10.7	15.8	17.7	23.7	26.1	26.8	22.1	14.7	11.9	5.1	15.8
1971	6.3	5.3	8.8	12.4	18.9	22.5	26.3	25.3	23.1	14.8	10.0	4.9	14.9
1972	2.1	2.9	9.0	14.7	17.2	21.6	24.4	25.2	22.1	16.8	9.0	3.3	14.1
1973	3.6	6.8	8.0	12.7	18.2	21.0	25.8	26.4	22.6	17.2	8.5	5.2	14.7
1974	2.3	5.8	11.1	12.4	17.9	23.4	27.2	25.1	20.3	17.9	10.0	5.4	15.0
1975	3.3	4.1	9.6	14.6	17.4	22.4	27.0	26.3	23.1	15.8	9.3	4.0	14.8
1976	3.8	3.0	8.7	12.6	17.5	22.8	24.3	24.9	21.1	16.1	10.7	6.8	14.4
1977	2.7	8.6	8.8	14.0	18.9	22.8	26.7	27.9	22.9	18.0	11.7	5.3	15.7
1978	5.7	7.4	9.8	13.0	20.2	22.8	28.4	25.9	22.4	18.1	8.9	7.1	15.9
1979	5.5	8.6	11.3	14.7	18.9	22.5	25.1	26.4	22.8	17.2	11.8	4.8	15.8
1980	2.2	5.2	8.4	12.7	17.9	24.0	27.9	27.5	22.9	17.1	11.9	7.8	15.5
1981	4.8	6.7	12.3	14.2	16.6	23.8	27.4	27.9	23.9	18.8	9.1	8.9	16.3
1982	6.1	4.0	7.9	14.1	18.4	23.6	25.2	26.2	23.4	16.3	9.0	5.1	15.0
TOTAL	160.3	226.3	366.0	564.9	773.6	973.8	1106.4	1120.0	968.3	722.8	463.4	254.5	644.5
MEAN	3.9	5.3	8.5	13.1	18.0	22.6	25.7	26.1	22.5	16.8	10.8	5.9	15.0
MAX	8.6	9.2	12.3	15.8	20.3	24.2	28.4	27.9	26.6	19.7	14.7	9.0	16.4
MIN	-1.0	-0.2	4.1	9.4	16.1	20.6	23.8	24.3	19.4	13.3	7.2	1.2	13.6

Fig. 6-20 Correlation between the Monthly Mean Temperature and Monthly Evaporation Values of Adana Meteorological Station

R= 0.929      COUNT= 280      6209 -      6612



Since observation of evaporation is done using Class-A-pans, the product of multiplication by a correction factor of 0.7 was taken to be the evaporation from the reservoir surface.

The results of calculations are given in Table 6-22.

(2) Gumusoren Reservoir

(a) Air Temperature

Since the elevation of the Gumusoren Reservoir (high water level 1,292 m) would be roughly the same as the elevation 1,400 m, of Tomarza Meteorological Station, it was decided to use the air temperature data of the Tomarza Station.

There is a good correlation between the monthly mean air temperatures at the Tomarza and Kayseri Stations with a correlation coefficient of 0.990, and the air temperatures at the Tomarza Station are supplemented by the following equation:

$$TTM = 1.01 * TKY - 1.77$$

where, TTM: monthly mean air temperature at the Tomarza Station (°C)

TKY: monthly mean air temperature at the Kayseri Station (°C)

The air temperatures at the Tomarza Station obtained in this manner are taken to be the air temperatures at the Gumusoren Reservoir Site.

(b) Evaporation

The values of evaporation observed by Class-A-pans at the Tomarza Meteorological Station were multiplied by the correction factor 0.7. The values thus obtained are taken to be the evaporation from the surface of the Gumusoren Reservoir.

For any period that the observed value of evaporation at Tomarza Meteorological Observatory is not available, the evaporation from the Gumusoren Reservoir surface is calculated by the following

equation using the correlation between monthly mean air temperature and monthly evaporation (correlation coefficient 0.925) at the Tomarza Station.

$$EGM = (10.80 * TGU - 33.02) * 0.7$$

where, EGU: monthly evaporation from the surface of the Gumusoren Reservoir (mm)

TGU: monthly mean air temperature at the Gumusoren Reservoir Site (°C)

The results of calculations are given in Table 6-23.

### (3) Bahcelik Reservoir

#### (a) Air Temperature

Since the elevation of the Bahcelik Reservoir (high water level 1,500 m) is roughly the same as the elevation 1,470 m, of the Pinarbasi Meteorological Station, it is decided to use the air temperature data of the Pinarbasi Station.

There is a good correlation between the monthly mean air temperatures at the Pinarbasi and Kayseri Station with a correlation coefficient of 0.991, and the air temperatures at the Pinarbasi Station are supplemented by the following equation:

$$TPN = 0.97 * TKY - 1.92$$

where, TPN: monthly mean air temperature at the Pinarbasi Station (°C)

TKY: monthly mean air temperature at the Kayseri Station (°C)

The air temperatures at the Pinarbasi station obtained in this manner are taken to be the air temperatures at the Bahcelik Reservoir Site.

(b) Evaporation

The correlation between monthly mean air temperature and monthly evaporation at the Tomarza Meteorological Station (correlation coefficient 0.925) is applied to the Bahcelik Reservoir site and the evaporation from the surface of Bahcelik Reservoir is calculated by the following equation:

$$EBA = (10.80 * TBA - 33.02) * 0.7$$

where, EBA: monthly evaporation from the surface of the Bahcelik Reservoir (mm)

TBA: monthly mean air temperature at the Bahcelik Reservoir Site (°C)

0.7: correction factor for Class-A-pan

The results of calculations are given in Table 6-24.



Table 6-22 Monthly Evaporation Values from the Goktas Reservoir (unit: mm)

YEAR	JAN	FEB	MAR	APR	MAY	JUN	JUL	AUG	SEP	OCT	NOV	DEC	TOTAL
1940	0.	0.	6.	52.	71.	112.	130.	132.	109.	79.	34.	3.	728.
1941	0.	6.	12.	53.	96.	116.	134.	136.	108.	56.	27.	0.	744.
1942	0.	0.	14.	43.	85.	125.	134.	132.	110.	74.	31.	0.	748.
1943	0.	0.	0.	29.	71.	101.	126.	143.	126.	90.	50.	3.	739.
1944	0.	0.	18.	51.	72.	111.	138.	131.	110.	81.	31.	0.	737.
1945	0.	0.	0.	31.	99.	114.	138.	142.	122.	71.	35.	0.	749.
1946	0.	0.	8.	50.	74.	114.	136.	142.	128.	63.	53.	3.	772.
1947	0.	0.	33.	55.	90.	115.	140.	141.	111.	75.	41.	6.	808.
1948	17.	14.	2.	59.	95.	124.	144.	146.	107.	64.	10.	0.	783.
1949	0.	0.	3.	22.	67.	109.	123.	130.	92.	72.	48.	0.	685.
1950	0.	0.	12.	65.	75.	108.	130.	130.	118.	64.	35.	8.	743.
1951	0.	0.	28.	52.	81.	112.	134.	139.	115.	57.	31.	0.	751.
1952	0.	0.	1.	46.	75.	110.	131.	140.	131.	88.	30.	15.	767.
1953	0.	0.	0.	39.	74.	112.	139.	139.	104.	74.	7.	0.	688.
1954	0.	0.	24.	33.	75.	119.	144.	147.	117.	82.	37.	2.	780.
1955	0.	13.	13.	44.	84.	126.	136.	130.	116.	92.	38.	1.	792.
1956	0.	0.	0.	45.	69.	118.	139.	146.	113.	68.	28.	0.	727.
1957	0.	0.	22.	48.	76.	123.	139.	146.	119.	95.	31.	0.	796.
1958	0.	0.	21.	46.	79.	109.	129.	142.	109.	72.	39.	3.	751.
1959	0.	0.	12.	53.	85.	106.	128.	132.	102.	60.	29.	5.	711.
1960	0.	0.	15.	49.	97.	114.	136.	138.	117.	90.	51.	20.	826.
1961	0.	0.	0.	53.	85.	116.	139.	143.	100.	73.	33.	7.	758.
1962	0.	0.	34.	43.	87.	117.	135.	146.	123.	82.	59.	9.	835.
1963	5.	11.	2.	48.	71.	111.	135.	142.	119.	84.	36.	0.	763.
1964	0.	0.	26.	44.	73.	111.	132.	135.	135.	83.	33.	2.	773.
1965	0.	0.	24.	42.	78.	123.	135.	136.	143.	50.	14.	3.	748.
1966	3.	21.	25.	56.	84.	121.	144.	149.	112.	78.	50.	7.	851.
1967	0.	0.	13.	55.	92.	107.	130.	130.	100.	72.	24.	7.	730.
1968	0.	0.	17.	67.	91.	115.	147.	127.	96.	67.	31.	3.	761.
1969	0.	0.	29.	32.	92.	121.	137.	146.	118.	74.	22.	5.	774.
1970	2.	10.	31.	67.	81.	123.	139.	144.	111.	59.	40.	0.	808.
1971	1.	0.	18.	43.	89.	114.	141.	141.	118.	60.	27.	0.	745.
1972	0.	0.	20.	59.	77.	108.	128.	133.	111.	74.	20.	0.	730.
1973	0.	4.	13.	45.	84.	104.	137.	142.	115.	77.	16.	0.	737.
1974	0.	0.	34.	43.	82.	121.	147.	132.	99.	82.	27.	0.	767.
1975	0.	0.	24.	59.	78.	114.	146.	141.	118.	67.	22.	0.	768.
1976	0.	0.	17.	45.	79.	116.	127.	131.	104.	69.	31.	4.	725.
1977	0.	17.	18.	55.	89.	116.	144.	152.	117.	83.	38.	0.	828.
1978	0.	8.	25.	48.	98.	116.	156.	138.	114.	83.	19.	6.	811.
1979	0.	17.	36.	59.	89.	114.	132.	142.	116.	77.	39.	0.	821.
1980	0.	0.	15.	45.	82.	125.	152.	149.	117.	76.	40.	11.	813.
1981	0.	3.	43.	56.	73.	123.	149.	152.	124.	88.	20.	19.	850.
1982	0.	0.	12.	55.	85.	122.	133.	140.	121.	71.	20.	0.	758.
TOTAL	27.	124.	737.	2087.	3551.	4955.	5885.	5986.	4916.	3194.	1375.	152.	32978.
MEAN	1.	3.	17.	49.	83.	115.	137.	139.	114.	74.	32.	4.	767.
MAX	17.	21.	43.	67.	99.	126.	156.	152.	143.	95.	59.	20.	851.
MIN	0.	0.	0.	22.	69.	101.	123.	127.	92.	50.	7.	0.	685.

Table 6-23 Monthly Evaporation Values from the Gumusoren Reservoir (unit: mm)

YEAR	JAN	FEB	MAR	APR	MAY	JUN	JUL	AUG	SEP	OCT	NOV	DEC	TOTAL
1940	0.	0.	0.	56.	72.	108.	140.	142.	93.	58.	15.	2.	686.
1941	0.	0.	0.	52.	101.	123.	144.	129.	95.	34.	0.	0.	678.
1942	0.	0.	0.	42.	99.	127.	130.	139.	86.	52.	9.	0.	675.
1943	0.	0.	0.	34.	75.	104.	126.	134.	96.	68.	21.	0.	658.
1944	0.	0.	11.	42.	67.	111.	130.	119.	88.	67.	10.	0.	644.
1945	0.	0.	0.	21.	85.	94.	129.	135.	96.	34.	7.	0.	606.
1946	0.	0.	0.	44.	74.	105.	133.	132.	102.	36.	23.	0.	650.
1947	0.	0.	25.	49.	88.	122.	142.	124.	87.	40.	21.	0.	699.
1948	0.	0.	0.	34.	78.	112.	137.	139.	92.	40.	0.	0.	623.
1949	0.	0.	0.	16.	90.	127.	140.	123.	77.	58.	21.	0.	653.
1950	0.	9.	0.	78.	80.	102.	130.	125.	121.	40.	15.	0.	700.
1951	0.	0.	28.	56.	79.	108.	136.	143.	103.	32.	11.	0.	696.
1952	0.	0.	0.	48.	73.	99.	133.	139.	121.	75.	15.	0.	703.
1953	0.	0.	0.	46.	74.	109.	135.	137.	91.	54.	0.	0.	647.
1954	0.	14.	1.	27.	86.	118.	152.	149.	103.	68.	20.	0.	723.
1955	0.	0.	14.	44.	85.	130.	145.	136.	108.	80.	11.	0.	747.
1956	0.	0.	0.	53.	67.	116.	134.	141.	79.	40.	0.	0.	630.
1957	0.	0.	6.	52.	74.	109.	144.	149.	123.	68.	0.	0.	726.
1958	0.	0.	18.	51.	86.	105.	133.	135.	94.	45.	8.	0.	674.
1959	0.	0.	0.	52.	86.	108.	142.	128.	80.	33.	6.	0.	635.
1960	0.	0.	5.	41.	94.	108.	142.	127.	105.	72.	28.	0.	723.
1961	0.	0.	0.	59.	101.	116.	138.	140.	74.	56.	12.	0.	695.
1962	0.	0.	28.	45.	90.	127.	156.	153.	104.	66.	34.	0.	807.
1963	0.	0.	0.	43.	72.	110.	136.	136.	101.	63.	9.	0.	649.
1964	0.	0.	14.	37.	74.	106.	136.	127.	91.	56.	13.	0.	655.
1965	0.	0.	6.	30.	63.	103.	120.	139.	103.	27.	4.	0.	596.
1966	0.	3.	5.	47.	71.	109.	136.	145.	93.	64.	42.	0.	717.
1967	0.	0.	0.	28.	74.	90.	114.	121.	89.	52.	0.	0.	567.
1968	0.	0.	0.	51.	80.	92.	130.	113.	84.	51.	16.	0.	618.
1969	0.	0.	3.	14.	77.	109.	114.	129.	95.	48.	0.	0.	588.
1970	0.	0.	11.	57.	68.	103.	133.	118.	85.	36.	21.	0.	630.
1971	0.	0.	2.	28.	71.	94.	130.	119.	100.	34.	5.	0.	581.
1972	0.	0.	0.	50.	68.	93.	130.	128.	103.	59.	0.	0.	631.
1973	0.	0.	0.	30.	74.	88.	125.	124.	96.	56.	0.	0.	592.
1974	0.	0.	14.	24.	74.	115.	127.	119.	80.	75.	9.	0.	627.
1975	0.	0.	0.	47.	67.	102.	136.	127.	93.	43.	0.	0.	615.
1976	0.	0.	0.	30.	69.	96.	114.	124.	83.	56.	18.	0.	589.
1977	0.	0.	0.	36.	71.	95.	122.	130.	96.	26.	20.	0.	595.
1978	0.	0.	9.	35.	80.	102.	136.	116.	95.	64.	0.	0.	638.
1979	0.	0.	13.	40.	78.	100.	118.	139.	107.	57.	23.	0.	675.
1980	0.	0.	0.	35.	74.	111.	147.	124.	89.	51.	6.	0.	636.
1981	0.	0.	14.	33.	52.	100.	131.	122.	102.	66.	0.	0.	622.
1982	0.	0.	0.	46.	74.	100.	112.	110.	94.	46.	0.	0.	590.
TOTAL	0.	25.	226.	1784.	3330.	4608.	5720.	5634.	4106.	2247.	473.	2.	28154.
MEAN	0.	1.	5.	41.	77.	107.	133.	131.	95.	52.	11.	0.	655.
MAX	0.	14.	28.	78.	101.	130.	156.	153.	123.	80.	42.	2.	807.
MIN	0.	0.	0.	14.	52.	86.	112.	113.	74.	26.	0.	0.	567.

Table 6-24 Monthly Evaporation Values from the Bahcecik Reservoir (unit: mm)

YEAR	JAN	FEB	MAR	APR	MAY	JUN	JUL	AUG	SEP	OCT	NOV	DEC	TOTAL
1940	0.	0.	0.	51.	67.	102.	132.	133.	87.	52.	12.	0.	635.
1941	0.	0.	0.	47.	94.	116.	136.	121.	99.	31.	0.	0.	634.
1942	0.	0.	0.	38.	83.	119.	123.	131.	80.	48.	0.	0.	628.
1943	0.	0.	0.	30.	69.	97.	118.	126.	90.	83.	18.	0.	611.
1944	0.	0.	8.	38.	62.	104.	122.	112.	82.	62.	7.	0.	596.
1945	0.	0.	0.	18.	82.	90.	121.	127.	90.	31.	4.	0.	562.
1946	0.	0.	0.	40.	68.	99.	124.	124.	96.	32.	19.	0.	602.
1947	0.	0.	21.	45.	82.	115.	133.	117.	81.	37.	18.	0.	649.
1948	0.	0.	0.	30.	72.	105.	129.	131.	86.	37.	0.	0.	590.
1949	0.	0.	0.	13.	83.	120.	132.	116.	71.	52.	18.	0.	607.
1950	0.	6.	0.	72.	74.	95.	122.	118.	114.	37.	12.	0.	649.
1951	0.	0.	25.	51.	73.	101.	127.	135.	96.	28.	8.	0.	644.
1952	0.	0.	0.	43.	68.	92.	125.	131.	114.	69.	12.	0.	654.
1953	0.	0.	0.	43.	68.	102.	127.	129.	85.	49.	0.	0.	603.
1954	0.	0.	0.	23.	80.	111.	143.	140.	96.	62.	0.	0.	673.
1955	0.	11.	11.	40.	79.	123.	137.	127.	101.	74.	8.	0.	711.
1956	0.	0.	0.	49.	62.	109.	126.	133.	73.	27.	0.	0.	597.
1957	0.	0.	3.	48.	68.	102.	136.	141.	116.	62.	0.	0.	676.
1958	0.	0.	15.	46.	80.	98.	124.	127.	90.	41.	5.	0.	627.
1959	0.	0.	0.	48.	80.	101.	134.	121.	74.	29.	3.	0.	589.
1960	0.	0.	2.	37.	88.	101.	134.	120.	98.	67.	25.	0.	671.
1961	0.	0.	0.	53.	94.	109.	130.	132.	68.	50.	9.	0.	645.
1962	0.	0.	24.	41.	86.	119.	147.	144.	102.	61.	30.	0.	751.
1963	0.	0.	0.	40.	67.	103.	114.	118.	88.	52.	7.	0.	588.
1964	0.	0.	2.	22.	61.	96.	122.	112.	78.	43.	0.	0.	537.
1965	0.	0.	3.	25.	65.	97.	119.	133.	93.	21.	0.	0.	556.
1966	0.	0.	2.	43.	60.	99.	124.	130.	84.	50.	35.	0.	634.
1967	0.	0.	0.	23.	66.	80.	102.	108.	80.	47.	0.	0.	507.
1968	0.	0.	0.	49.	80.	87.	121.	104.	81.	50.	15.	0.	587.
1969	0.	0.	0.	16.	77.	102.	107.	121.	85.	45.	0.	0.	553.
1970	0.	0.	10.	56.	63.	96.	121.	108.	79.	34.	19.	0.	587.
1971	0.	0.	2.	28.	74.	88.	124.	110.	96.	29.	4.	0.	556.
1972	0.	0.	0.	52.	65.	88.	127.	121.	89.	56.	0.	0.	598.
1973	0.	0.	0.	31.	69.	85.	118.	116.	86.	51.	0.	0.	556.
1974	0.	0.	11.	18.	73.	115.	121.	114.	73.	74.	6.	0.	608.
1975	0.	0.	0.	45.	65.	96.	130.	120.	87.	37.	0.	0.	581.
1976	0.	0.	0.	31.	68.	96.	113.	112.	74.	52.	21.	0.	570.
1977	0.	0.	0.	39.	68.	93.	121.	134.	92.	21.	12.	0.	579.
1978	0.	0.	0.	24.	70.	96.	136.	110.	83.	66.	0.	0.	584.
1979	0.	0.	18.	50.	82.	101.	119.	145.	111.	60.	34.	0.	719.
1980	0.	0.	0.	36.	78.	106.	144.	121.	89.	50.	0.	0.	621.
1981	0.	0.	0.	22.	42.	90.	127.	120.	103.	67.	0.	0.	571.
1982	0.	0.	0.	39.	70.	100.	111.	118.	84.	36.	0.	0.	558.
TOTAL	0.	17.	156.	1633.	3128.	4343.	5405.	5308.	3815.	2053.	384.	0.	26242.
MEAN	0.	0.	4.	38.	73.	101.	126.	123.	89.	48.	9.	0.	610.
MAX	0.	11.	25.	72.	94.	123.	147.	145.	116.	74.	35.	0.	751.
MIN	0.	0.	0.	13.	42.	80.	102.	104.	68.	21.	0.	0.	507.

## 6.4 Sedimentation in Reservoir

### 6.4.1 Data Used for Estimation of Sedimentation

Sediment carried down a river is divided into suspended load and bed load according to the form of transport. With regard to suspended load, the observation technique using sampling has been established and observations are widely being carried out in Turkey by EIE and others. However, observations of bed load are difficult to perform on actual streams, and the situation at present is that estimates must be relied on.

When calculating the design sedimentation of a reservoir, observation data of suspended load in the vicinity of the project site and data of actual sedimentation in existing reservoirs, are generally used. If case data from observations within the catchment area are not available, observation records of neighboring streams of similar characteristic are used at times.

For the Seyhan River Basin, the observation data of the runoff gauging stations of EIE listed in Table 6-25 can be utilized. The suspended load observation data obtained by EIE on neighboring rivers such as the Ceyhan River running down on the east side of the Seyhan River also can be utilized. Actual sedimentation data of the existing Seyhan Dam reservoir exist, but in this connection there is a landslide zone in the basin of the tributary Cakit River, feeding Seyhan Reservoir with a substantial amount of sediment supplied from this zone, so that the sedimentation recorded at Seyhan Reservoir is of an abnormally large value compared with the sediment supply calculated from the observed data at the No. 1818 Gaging Station. Therefore, it was chosen not to use the sedimentation data of Seyhan Reservoir.

## 6.4.2 Estimation of Sediment Weight Deposited in Reservoir

### (1) Suspended Load

EIE has calculated annual suspended loads at various observation sites using the correlations between river discharges and suspended loads obtained from results of observations on suspended sediment. These values are given in Table 6-25. The results of plotting relationships, between catchment areas and annual suspended loads (ton/yr), including the values at observation points on rivers neighboring the Seyhan such as the Ceyhan River, are shown in Fig. 6-21. This figure shows that there is a correlation between annual suspended load and catchment area and the following equation was obtained:

$$\log SL = 0.09356 + 1.58078 * \log A$$

where, SL: annual suspended load (ton/yr)

A: catchment area (km<sup>2</sup>)

Since observation data were not available on the Zamanti River, the above equation was applied to the Goktas and Gumusoren dam sites and the annual suspended loads at these sites were obtained. The results are given below.

Goktas dam site (8,290 km<sup>2</sup>) : 1,261,000 ton/yr (152 ton/yr/km<sup>2</sup>)  
Gumusoren dam site (6,325 km<sup>2</sup>) : 822,000 ton/yr (130 ton/yr/km<sup>2</sup>)

These values are of an order equivalent to the value (190 ton/yr/km<sup>2</sup>) calculated by Fleming's method.

### (2) Bed Load

A method of measuring bed load has not been established as yet, and in general, it is expressed by the ratio to suspended Load. This ratio is said to be 5 to 10 percent in a plain area and 10 to 30 percent in a mountain area. In this case, taking into consideration the topography of the Zamanti River Basin, the ratio of bed load is estimated to be 12 percent of suspended load.

(3) Trapping Ratio

Brune has given the relationship between trapping ratio and a value of (total reservoir capacity)/(total annual inflow). On calculating the values of (total reservoir capacity)/(total annual inflow) for Goktas Reservoir and Gumusoren Reservoir, they are as follows:

$$\begin{aligned} \text{Goktas Reservoir} & : (109.33 \times 10^6 / 1,703.9 \times 10^6) * 100 = 6.4\% \\ \text{Gumusoren Reservoir} & : (138.90 \times 10^6 / 572.5 \times 10^6) * 100 = 24.0\% \end{aligned}$$

The sediment trapping ratios of Goktas Reservoir and Gumusoren Reservoir obtained from Brune's diagram using these values are 80 percent and 95 percent, respectively.

(4) Design Sedimentation of Goktas Reservoir by Weight

The design sedimentation (weight) of Goktas Reservoir is to be calculated by the equation below using the annual suspended load (ton/yr), bed load ratio (%), and trapping ratio (%) obtained in paragraphs (1), (2), and (3) above.

$$SW_t = S_L * (1 + E_{b1}/100) + (E_t/100) * t$$

where,  $SW_t$ : reservoir sedimentation by weight (ton)

$S_L$ : annual sedimentation (ton/yr)

$E_{b1}$ : bed load ratio (%)

$E_t$ : trapping ratio (%)

$t$ : period (yr)

The length of the period for calculation of design sedimentation was taken to be 50 years. Regarding the timing of completion of Gumusoren Dam planned upstream of Goktas Reservoir, the six cases of before completion of Goktas Dam, 10 years after, 20 years after, 30 years after, 40 years after, and 50 years after were considered and the 50-years sedimentation (weight) in Goktas Reservoir for each of the cases was calculated. The results of the calculations are included in Table 6-26.

### 6.4.3 Estimation of Sediment Volume of Reservoir

#### (1) Sediment Density

It is necessary to calculate the volume of sediment, deposited in a reservoir considering the density after deposition. According to Lane and Koelzer, the average sediment density  $W_t$  (ton/m<sup>3</sup>) after elapse of time  $t$  may be obtained by the equation below.

$$W_t = W_1 + K * \left( \frac{t}{t-1} * (\log_e t - 1) \right)$$

where,  $W_1$ : initial density (ton/m<sup>3</sup>)  
 $K$ : consolidation coefficient

The values of initial density  $W_1$  and consolidation coefficient  $K$  will differ depending on composition of the sediment and operating conditions of the reservoir. In the case here, the values in the table below are selected considering the results of analyzing samples from the suspended load observation station and the operating conditions of Goktas Reservoir.

Component	Sand	Silt	Clay
Component ratio (%)	30	40	30
$W_1$ (ton/yr)	1.426	1.115	0.048
$K$ (ton/yr)	0	0.0188	0.0744

As a result, the average sediment density of Goktas Reservoir 50 years later was calculated as 0.977 ton/m<sup>3</sup>.

#### (2) Design Sediment Volume of Goktas Reservoir

The design sedimentation volume  $SV_{50}$  (m<sup>3</sup>) of Goktas Reservoir is to be calculated by the equation below using the weight of sediment  $SW_{50}$  (ton) during the period of 50 years and average sediment density in after 50 years  $W_{50}$  (ton/m<sup>3</sup>) obtained in the foregoing.

$$SV_{50} = SW_{50}/W_{50}$$

The results of calculations for the six cases considering the timing of completion of Gumusoren Dam are included in Table 6-26.

Fig.6-21 CORRELATION BETWEEN THE SUSPENDED SEDIMENT YIELD AND THE SIZE OF CATCHMENT AREA

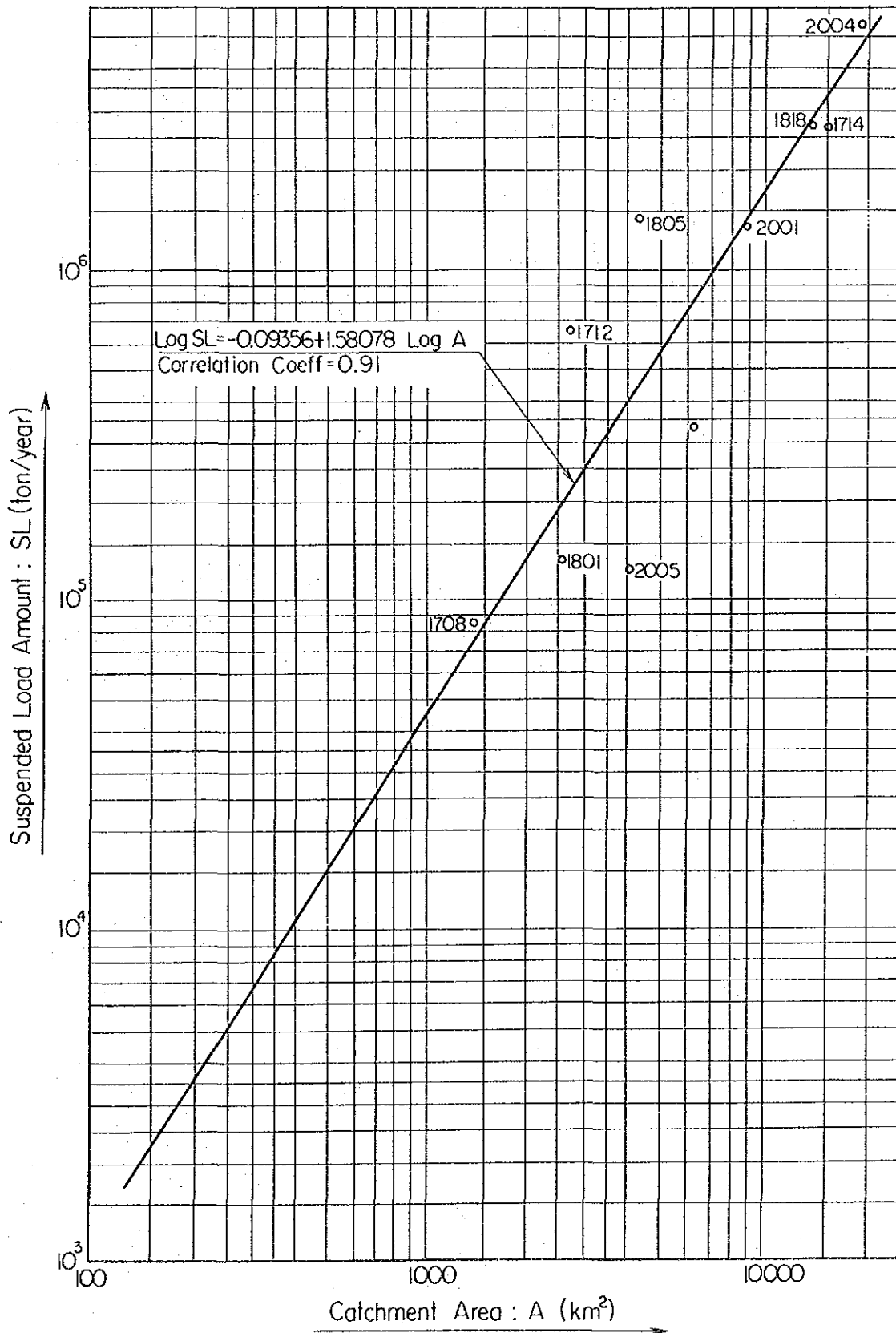




**Table 6-25 Suspended Sediment Data of the Gauging Stations within the Seyhan River Basin**

Station	River	Catchment Area (km <sup>2</sup> )	Observation Period	Number of Samples	Annual Mean Sediment Yield (ton/year/km <sup>2</sup> )
1801 Himmetli	Goksu	2,563	1966 - 1984	107	51
1805 Gokdere	Goksu	4,243		12	344
1818 Uctepeler	Seyhan	14,015	1968 - 1984	113	191
Bakirdag	Zamanti	6,158		118	54

**Table 6-26 50 Years Sediment Amounts for the Goktas Reservoir**

Completion Timing of the Gumusoren Dam to the Goktas Dam	Sediment Values	
	Weight (10 <sup>3</sup> ton/50 years)	Volume (10 <sup>3</sup> m <sup>3</sup> /50 years)
50 years after Goktas Dam	56,490	57,820
40 years after Goktas Dam	49,500	50,670
30 years after Goktas Dam	42,500	43,500
20 years after Goktas Dam	35,500	36,340
10 years after Goktas Dam	28,510	29,180
before Goktas Dam	21,510	22,020

## 6.5 Probable Flood Discharge

### 6.5.1 Data used for Calculating Probable Flood Discharge

- (1) The observation data from the runoff gauging stations of EIE listed in Table 6-2 are available as flood discharge observation data in the Zamanti River Basin and its surroundings. Of these data, the ones that are directly related to calculation of flood discharge at the Goktas dam site are those from the No. 1806 Gauging Station downstream of the dam site and the Nos. 1802 and 1822 Gauging Stations upstream. However, concerning the No. 1802 station, peak discharge observations have not been made and only interval flood discharge records are available there. The flood observation data of the No. 1805 Gaging Station on the Goksu River and the No. 1818 Gaging Station on the Seyhan River will serve as references in finding the will serve as references in finding the relationship between floods in the Zamanti River Basin and in the Gokusu River Basin.

The yearly maximum peak discharges at the gauging stations Nos. 1822, 1806, 1805, and 1818, and the maximum discharge records at the No. 1802 Gaging Station, and the dates of occurrence of those discharges are given in Table 6-27. According to Table 6-27, flood discharges at the No. 1806 Gauging Station site (catchment area 8698 km<sup>2</sup>) are double to triple those at the No. 1802 Gauging Station site (catchment are 8,418 km<sup>2</sup>). This indicates that the discharge from the area downstream of the No. 1802 Gauging Station greatly influences the flood discharge at the Goktas dam site (catchment area 8,290 km<sup>2</sup>). Therefore, in calculation of the probable flood discharge at the Goktas dam site, it was decided to calculate the probable flood discharges at the No. 1806 Gauging Station site and convert them it to the discharge at the dam site.

Observation data of the No. 1806 Gauging Station are missing for the 4-year period of the 1957 to 1960 hydrological years, s and since the 1981 hydrological year. Consequently, the annual maximum peak discharges for these years were supplemented using the observation data of the No. 1805 and 1818 Gauging Station. The method of supplementation is mentioned in Table 6-27.

Table 6-27 Flood Peak Discharge Values at Nos. 1806, 1802, 1822, 1805, and 1818 G.S.

Water Year	Station Numbers (Catchment Area)									
	1806 (8,698 km <sup>2</sup> )		1802 (7,418 km <sup>2</sup> )		1822 (6,335 km <sup>2</sup> )		1805 (4,243 km <sup>2</sup> )		1818 (13,846 km <sup>2</sup> )	
	Date	Discharge (m <sup>3</sup> /s)	Date	Discharge (m <sup>3</sup> /s)	Date	Discharge (m <sup>3</sup> /s)	Date	Discharge (m <sup>3</sup> /s)	Date	Discharge (m <sup>3</sup> /s)
1939	28 Apr.	214.1	27 Apr.	92.7	17 Mar.	590.6	17 Mar.	590.6	discharge observation started from 1966 w.y.	
1940	3 Apr.	382.0	3 Apr.	156.0	3 Apr.	567.4	3 Apr.	567.4		
1941	1 Mar.	203.2	15 Apr.	88.5	29 Jan.	578.2	29 Jan.	578.2		
1942	4 Apr.	271.8	5 Apr.	96.9	2 Apr.	464.8	2 Apr.	464.8		
1943	20 Nov.	319.0	7 Apr.	126.0	5 Apr.	569.6	5 Apr.	569.6		
1944	28 Mar.	335.8	2 May	88.5	28 Mar.	678.4	28 Mar.	678.4		
1945	8 Apr.	182.0	7 May	67.7	7 Apr.	198.8	7 Apr.	198.8		
1946	10 May	192.2	3 May	67.7	15 Feb.	550.9	15 Feb.	550.9		
1947	30 Mar.	140.6	30 May	51.2	14 Mar.	443.2	14 Mar.	443.2		
1948	28 Nov.	340.0	11 Apr.	84.0	27 Nov.	826.4	27 Nov.	826.4		
1949	24 Mar.	276.0	3 May	67.7	19 Apr.	440.5	19 Apr.	440.5		
1950	6 Mar.	289.0	15 May	75.5	6 Mar.	385.0	6 Mar.	385.0		
1951	25 Mar.	190.0	27 Apr.	52.0	21 Jan.	543.0	21 Jan.	543.0		
1952	3 Apr.	327.4	3 Apr.	140.0	13 Dec.	670.0	13 Dec.	670.0		
1953	11 Apr.	329.5	15 Apr.	107.4	4 Apr.	543.0	4 Apr.	543.0		
1954	26 Apr.	276.0	25 Apr.	123.0	20 Jan.	719.0	20 Jan.	719.0		

- Continue -

Water Year	1806 (8,698 km <sup>2</sup> )		1802 (7,418 km <sup>2</sup> )		1822 (6,335 km <sup>2</sup> )		1805 (4,243 km <sup>2</sup> )		1818 (13,846 km <sup>2</sup> )	
	Date	Discharge (m <sup>3</sup> /s)	Date	Discharge (m <sup>3</sup> /s)	Date	Discharge (m <sup>3</sup> /s)	Date	Discharge (m <sup>3</sup> /s)	Date	Discharge (m <sup>3</sup> /s)
1955	27 Dec.	224.6	out of operation				31 Jul.	801.0		
1956	27 Apr.	167.9					4 Feb.	410.8		
1957	-	482.0					3 Mar.	926.0		
1958	-	627.0					9 Jan.	1,187.4	10 Jan.	2,179.0
1959	-	297.0					15 Apr.	464.8		The value of 1958 was calculated from the value of No. 1814 G.S.
1960	-	314.0					26 Apr.	503.4		
1961	13 Apr.	103.0					6 Feb.	158.0		
1962	18 Mar.	202.0					17 Dec.	675.0		
1963	19 Dec.	970.0					19 Dec.	1,440.0		
1964	26 Mar.	151.0					25 Mar.	198.0		
1965	28 Mar.	253.0					18 Apr.	485.0		
1966	25 Jan.	363.0					5 Jan.	1,150.0	5 Jan.	1,700.0
1967	16 Dec.	279.0					16 Dec.	570.0	16 Dec.	1,046.0
1968	14 Mar.	249.0					14 Mar.	870.0	14 Mar.	1,224.0
1969	18 Mar.	313.0					28 Dec.	676.0	26 Dec.	1,331.0
1970	18 Dec.	277.0				14 Apr.	65.4	18 Dec.	18 Dec.	1,258.0
1971	17 Apr.	180.0			15 Apr.	54.4	17 Apr.	330.0	17 Apr.	705.0

- Continue -

Water Year	1806 (8,698 km <sup>2</sup> )		1802 (7,418 km <sup>2</sup> )		1822 (6,335 km <sup>2</sup> )		1805 (4,243 km <sup>2</sup> )		1818 (13,846 km <sup>2</sup> )		
	Date	Discharge (m <sup>3</sup> /s)	Date	Discharge (m <sup>3</sup> /s)	Date	Discharge (m <sup>3</sup> /s)	Date	Discharge (m <sup>3</sup> /s)	Date	Discharge (m <sup>3</sup> /s)	
1972	30 Apr.	330.0	out of operation		30 Apr.	81.5	30 Apr.	461.0	30 Apr.	672.0	
1973	26 Feb.	154.0			13 Mar.	62.1	26 Feb.	253.0	27 Feb.	405.0	
1974	15 Mar.	283.0			15 Mar.	79.0	15 Mar.	386.0	15 Mar.	934.0	
1975	29 Apr.	789.0			26 Apr.	108.0	29 Apr.	1,043.0	29 Apr.	1,957.0	
1976	12 Apr.	190.0			12 Apr.	77.7	12 Apr.	510.0	13 Apr.	759.0	
1977	23 Apr.	372.0			23 Apr.	105.0	23 Apr.	608.0	23 Apr.	1,205.0	
1978	1 Jan.	201.0			10 Apr.	68.2	1 Jan.	450.0	2 Jan.	988.0	
1979	3 Jan.	519.0			3 Jan.	97.8	3 Jan.	1,963.0	3 Jan.	3,278.0	
1980	29 Mar.	576.0			27 Mar.	185.0	28 Mar.	1,551.0	-	-	
1981	-	503.0			20 Mar.	86.5	6 Jan.	648.0	6 Jan.	1,409.0	
1982	-	707.0			5 Apr.	115.0	16 Dec.	906.0	16 Dec.	1,947.0	
1983	-	226.0			31 Mar.	79.8	29 Mar.	322.0	29 Mar.	692.0	
Remarks	<p>* No. 1806 G.S. peak discharge values of 1957 - 1960 and 1981 - 1983 w.y. were supplemented with the following regression equation of correlation between the peak discharge values of No. 1806 and No. 1805 G.S., or between (No. 1806 + No. 1805) and No. 1818 G.S. determined by using the peak discharge values recorded in same date.</p> <p>1957, 1959, 1960 : Qp1806 = 10** (0.70472 * logQp1805 + 0.59257) (R = 0.916)</p> <p>1958, 1981, 1982, 1983: Qp1806 = 10** (1.0442 * logQp1818 - 0.22712) - Qp1805 (R = 0.968)</p> <p>* The discharge values of No. 1802 G.S. are not real peak discharge value. They are maximum values of the interval records.</p>										

## 6.5.2 Calculation of Probable Flood Discharge at Project Site

### (1) Probable Flood Discharge at the No. 1806 Gauging Station Site

Analyses were performed using the annual maximum peak discharge data for the 45-year period from the 1939 to the 1983 hydrological year given in Table 6-27.

Firstly, as a result of carrying out verifications of the data by Chi-square tests, it was indicated that a distribution conforming to a distribution function of a logarithmic Pearson III type. Accordingly, the probable flood discharge was calculated adopting the logarithmic Pearson III type distribution function. Also, though the distribution function was not appropriate, calculation by the Gumbel distribution widely used in general was done for the sake of reference. The results of these calculations are shown in Table 6-28 and Fig. 6-22.

### (2) Probable Flood Discharge at the Goktas Dam Site

As stated in the preceding section (6.5.1), an abrupt change in runoff is seen at the downstream most part of the Zamanti River even during a flood. Therefore, the flood discharge at the Goktas dam site is to be estimated with consideration of this runoff variation. since data of peak discharges did not exist for the No. 1802 Gauging Station, the relationship between the peak discharges from the same flood at the No. 1822 Gauging Station site (catchment area 6,335 km<sup>2</sup>) further upstream and the No. 1806 Gauging Station site (catchment area 8,698 km<sup>2</sup>) was examined using the equation below.

$$\frac{FQ_{1822}}{FQ_{1806}} = \left( \frac{A_{1822}}{A_{1806}} \right)^n = \left( \frac{6335 \text{ km}^2}{8698 \text{ km}^2} \right)^n$$

As a result, values of n fell in a range of 2.82 to 6.27, and using n = 2.82 which is on the most conservative side in converting from the discharge at the No. 1806 Gauging Station site, the following equation is to be taken:

$$FQ_{1822} = \left( \frac{6335 \text{ km}^2}{8698 \text{ km}^2} \right)^{2.82} * FQ_{1806} = 0.409 * FQ_{1806}$$

Then, the flood discharge at the Goktas Dam Site is obtained by the following equation with hypothesis that discharge increase with increase in catchment area for the section of the river between the No. 1822 and the No. 1806 gauging station:

$$\begin{aligned}
 FQ_{DAM} &= FQ_{1822} + (FQ_{1806} - FQ_{1822}) * \frac{A_{DAM} - A_{1822}}{A_{1806} - A_{1822}} \\
 &= FQ_{1822} + (FQ_{1806} - FQ_{1822}) * \frac{8290 - 6335}{8698 - 6335} \\
 &= 0.1727 * FQ_{1822} + 0.8273 * FQ_{1806}
 \end{aligned}$$

Substituting the relationship between  $FQ_{1822}$  and  $FQ_{1806}$  previously determined in the above equation, the following equation is obtained:

$$\begin{aligned}
 FQ_{DAM} &= 0.1727 * (0.409 * FQ_{1806}) + 0.8273 * FQ_{1806} \\
 &= 0.898 * FQ_{1806}
 \end{aligned}$$

The probable flood discharges of any return period at the Goktas dam site are obtained converting the probable flood discharge at the No. 1806 Gauging Station site using the above equation. The result is given in Table 6-28.

(2) Probable Flood Discharge at the Goktas Powerhouse site

The catchment area of the Zamanti River at the Goktas powerhouse site was calculated as 8,700 km<sup>2</sup>. This figure is almost equal to the catchment area of 8,698 km<sup>2</sup> of the No. 1806 Gauging Station site. Consequently, the flood discharges at the Goktas powerhouse site are considered to be equal to that at the No. 1806 Gauging Station site.

Fig. 6-22 FREQUENCY ANALYSIS OF THE PEAK DISCHARGE SERIES OF No. 1806 G. S.

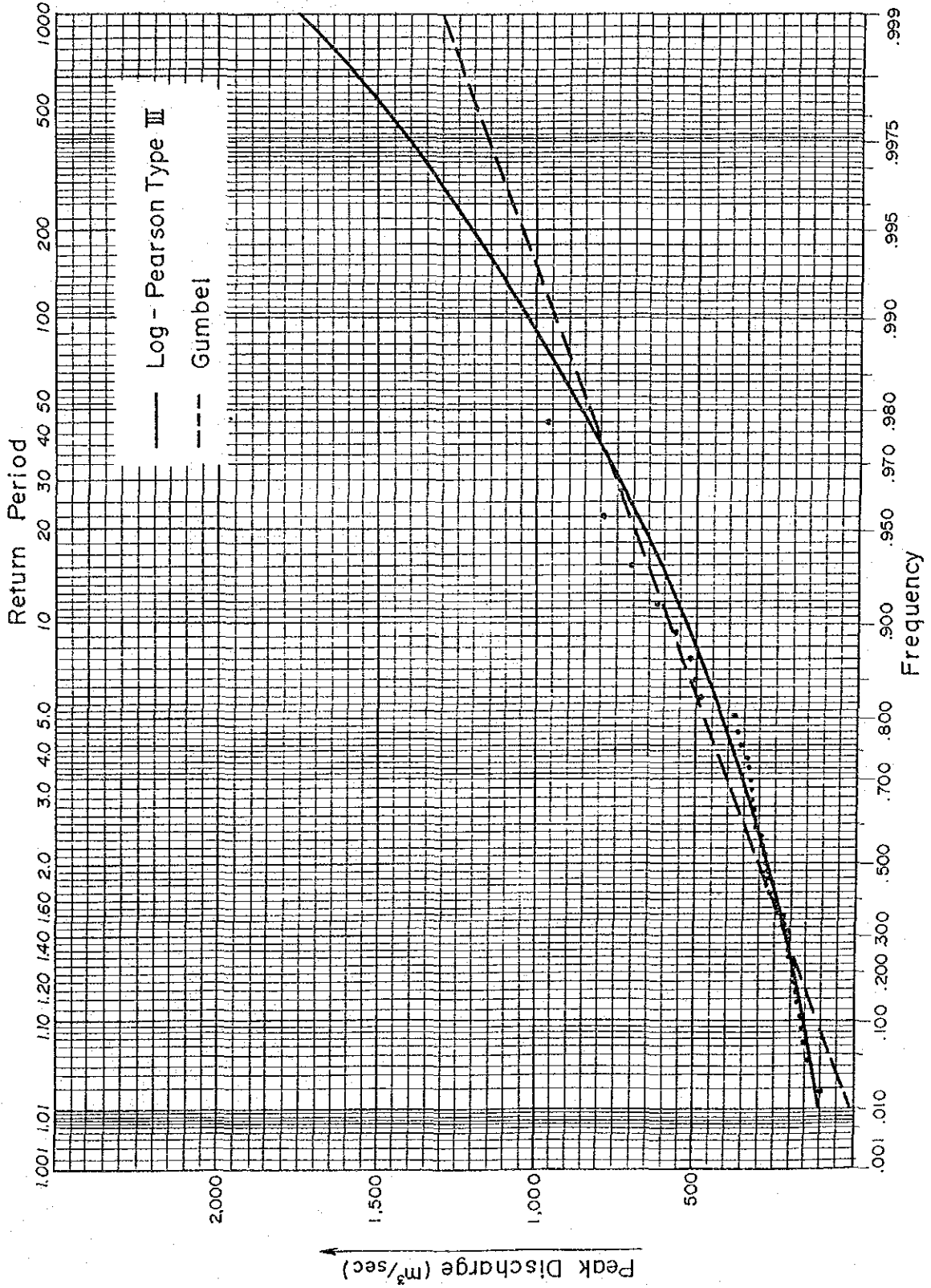




Table 6-28 Various Return Period Peak Discharge Values at the No. 1806 G.S. and the Goktas Damsite

Distribution Function	Return Periods (Years)	Peak Discharge Values (m <sup>3</sup> /s)		Remark	
		No. 1806 G.S (8,698 km <sup>2</sup> )	Goktas Damsite (8,290 km <sup>2</sup> )		
Log Pearson Type III Distribution	5	422	379	* FQDAM = 0.898 * FQ1806 * Peak discharge values at the Goktas Powerhouse site can be considered to be the same values as at No. 1806 G.S., because the powerhouse site is very close to the No. 1806 G.S. site.	
	10	539	484		
	25	712	639		
	50	860	772		
	100	1,028	923		
	200	1,216	1,092		
	1,000	1,755	1,576		
	10,000	2,828	2,540		
	Gumbel Distribution	5	471		423
		10	585		525
25		730	656		
50		837	752		
100		943	847		
200		1,049	942		
1,000		1,295	1,163		
10,000		1,646	1,478		

## 6.6 Probable Maximum Flood (PMF) Discharge

### 6.6.1 Data used for Probable Maximum Flood

#### (1) Historical Storm

Observation data on such items as precipitation, vapor pressure, air temperature, etc. required for PMF analysis are adequate for utilization since 1963 in case of the Zamanti River Basin as can be comprehended from Table 6-1. Therefore, in PMF analysis for the Goktas dam site, major storms which occurred in the basin during the period from 1963 to 1986 were selected, and analyses were made on these storms. The selected historical are listed in Table 6-29.

#### (2) Rainfall during period of Storm

Storms in the Zamanti River Basin occur due to atmospheric lows which approach from the Mediterranean Sea direction in the rainy season from November to May. Moist air masses transported by atmospheric lows strike against the Tros Mountain Range at the northern end of the Mediterranean climate region, and after releasing large amounts of rain on the area south of the mountain range, cross over the mountains to enter the Central Anatolian Region. Consequently, compared with the area on the south side of the Tros Mountain Range, there is little rainfall due to storms in the Central Anatolian Region.

Since the basin of the Goktas dam site is mostly belong to the central Anatolian Region, there is a little amount of precipitation during storm as average of the whole basin.

However, the downstream most part of the river basin is located on the south side of the Tros Mountain Range and the rainfall during a period of storm is of a considerable amount. Accordingly, rainfall in this area has a great influence on the flood discharge of the Lower Zamanti River Basin and is an important factor in calculation of PMF at the Goktas dam site. However, since there is no meteorological station in this part of the basin, the rainfall data of the Mansurlu Meteorological Station closest to the site is selected to use its rainfall data as representative of this area.

Hence, the rainfall data of 15 meteorological stations, adding the Mansurlu Meteorological station to the 14 station within the catchment area listed in Table 6-1, are used for the calculation of rainfall during a storm in the basin of the Goktas Dam site.

Since rainfall durations of major storms in the Zamanti River Basin are longer than 24 hours, precipitation data in units of days are used for analyses.

(3) Precipitable Water

Precipitable water used for maximizing a storm is expressed as a function of dew-point temperature, but in Turkey, vapor pressure is being observed as an alternative to dew-point temperature. Vapor pressures are being measured also in the basin of the Goktas Dam site and its surroundings at some meteorological stations as shown in Table 6-1. The precipitable water is calculated using the data of the stations of Tomarza and Pinarbasi in the basin of the Goktas Dam site and Sariz, Develi, and Kozan in the surroundings.

(4) Probable Maximum Snowmelt (PMSM)

As mentioned in 6.1.3, there is a fair amount of snow cover resulting in the basin of the Goktas Dam site in winter time, which melts to discharge water in March to May as the temperature rises. On looking at the annual maximum peak discharges at the No. 1806 Gauging Station listed in Table 6-27, years in which floods occurred in March and April are most numerous. In this way, the discharge from snowmelt is a major factor in floods occurring in the Zamanti River Basin. Therefore, in calculating PMF at the Goktas dam site, it is necessary to consider the probable maximum snowmelt (PMSM). As observation data of air temperature used for calculating PMSM, the data of the Pinarbasi station located in roughly the middle of the catchment area is selected to use as representative of the Goktas dam basin.

## 6.6.2 Calculation of Probable Maximum Precipitation

### (1) Actual Precipitation during Storms

In the catchment area of Goktas Dam site, as stated in 6.6.1 (2), there is a great difference of precipitation amount between the middle-to-upper basin and the lower basin with the Tros Mountain Range as the boundary. Accordingly, the basin is divided into two parts and the average rainfall of each part is obtained respectively. That is, the average precipitation amount  $P_1$  of meteorological stations in the basin represents the middle and upper basin (area:  $A_1$  km<sup>2</sup>), while the precipitation amount  $P_2$  of Mansurlu Meteorological station represents the lower basin (area:  $A_2$  km<sup>2</sup>). The average rainfall  $P_{ave}$  of the entire basin is calculated by the following equation using the representative rainfalls of the two parts of the basin:

$$P_{ave} = \frac{P_1 * A_1 + P_2 * A_2}{A_1 + A_2} \quad (\text{mm})$$

In the analyses here, 90% and 10% are used as the values of  $A_1$  and  $A_2$  for the estimation of  $P_{ave}$  under consideration of topography, vegetation, etc. of the Goktas Dam basin.

### (2) Maximization of Storms

Maximization of a storm in PMP analysis is done by multiplication of the actual precipitation during the storm by the ratio of the maximum precipitable water  $W_m$  (mm) for the precipitable water  $W_s$  (mm) during the storm.

Since for the Goktas Dam basin, the Tros Mountain Range acts as a topographical barrier to moist air masses moving in from the Mediterranean Sea, precipitable water is calculated with the average elevation 1,600 m of the mountain range taken as the bottom surface of the air column. That is, the value of precipitable water is that of an air column with 1,000 mb as the bottom and 200 mb as the top from which that of an air column with similarly 1,000 mb as the bottom and EL. 1,600 m as the top is deducted.

The precipitable water  $W_s$  during the storm is estimated using the average value of the 12-hour 1,000-mb dew-point temperatures obtained from the 12-hour vapor pressures of the 5 stations mentioned in the preceding section 6.6.1 (3). And the maximum precipitable water  $W_m$  is estimated using the average values of probable maximum 12-hour 1,000-mb dew-point temperatures of the individual stations obtained from the probable maximum 12-hour vapor pressures during the storm, which obtained using the envelopes of monthly maximum 12-hour vapor pressures at the meteorological stations shown in Figs. 6-23 (1) to (5). With regard to the value of probable maximum 12-hour vapor pressure, the 15-day periods before and after the period of storm were considered as being of the same period from a seasonal point of view, and the maximum value during the period was used.

Maximization of the individual storms was done using the  $W_s$  and  $W_m$  values of the storms obtained in the abovementioned manner, and its results are shown in Table 6-29. Of these, the maximization of the storm of March 1980 yielding the probable maximum 24-hour precipitation is shown in Table 6-30. The depth-duration curve of PMP obtained from the result of the maximization given in Table 6-29 is shown in Fig. 6-24.

Fig. 6-23 Enveloping Curves of Maximum Vapor Pressure Values Observed at Tomarza, Pinarbasi, Sariz, Deveri and Kozan Meterological Stations

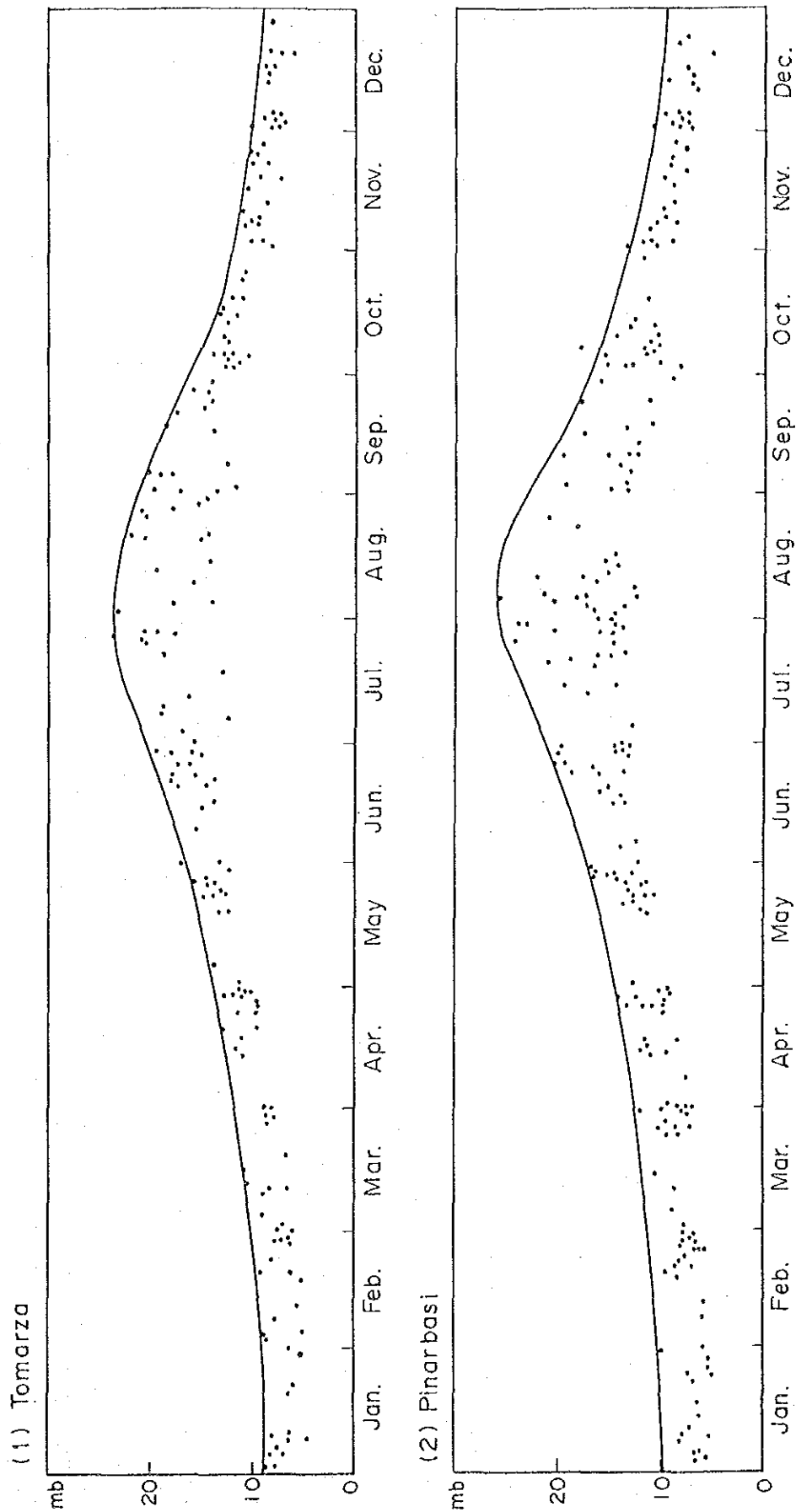


Fig. 6-23 - Continue -

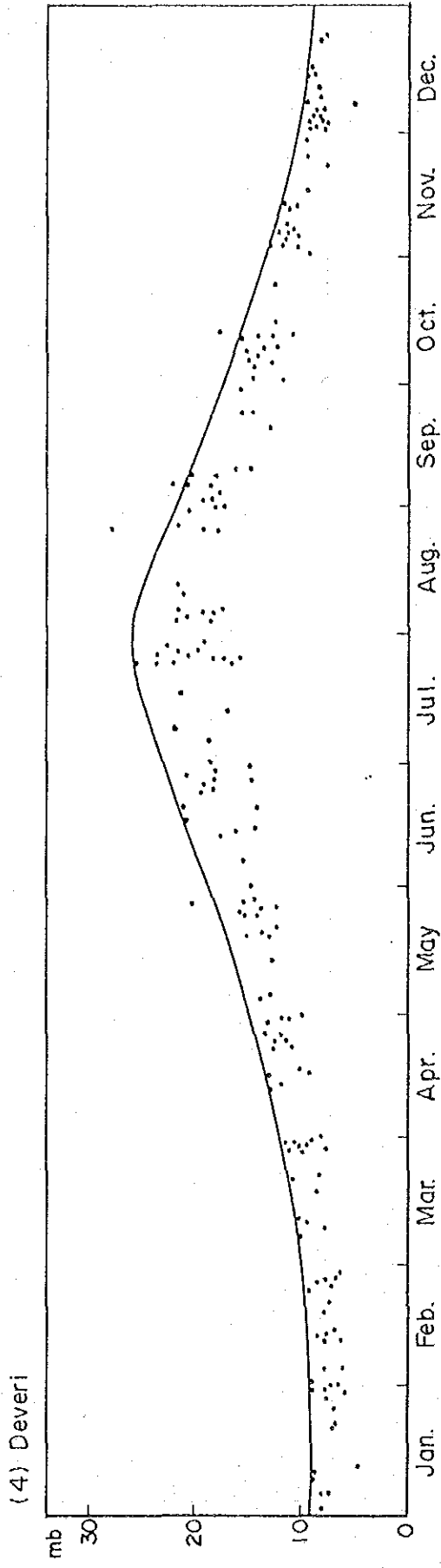
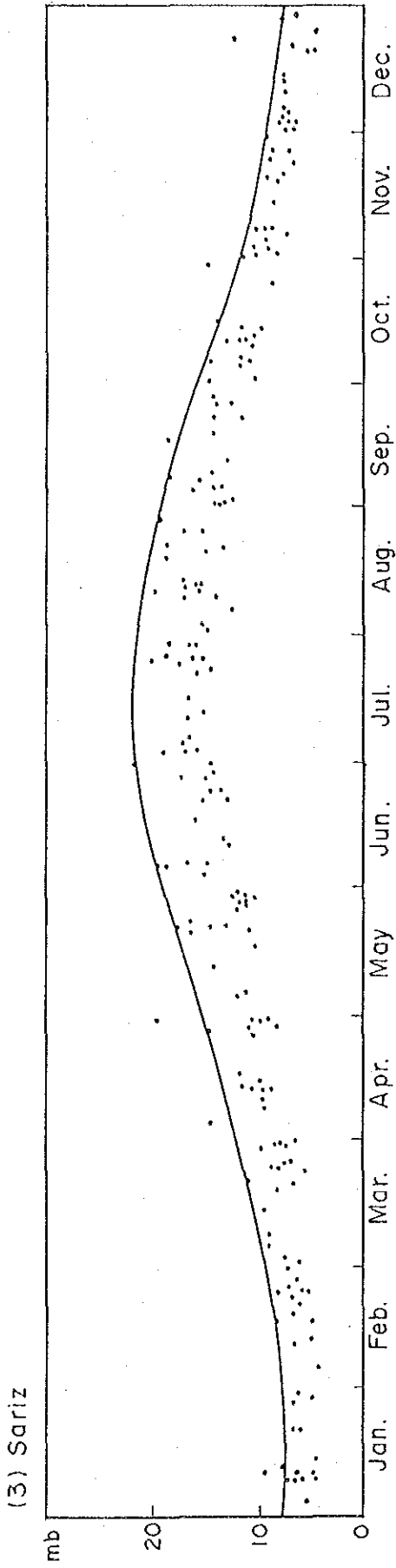


Fig. 6-23 — Continue —

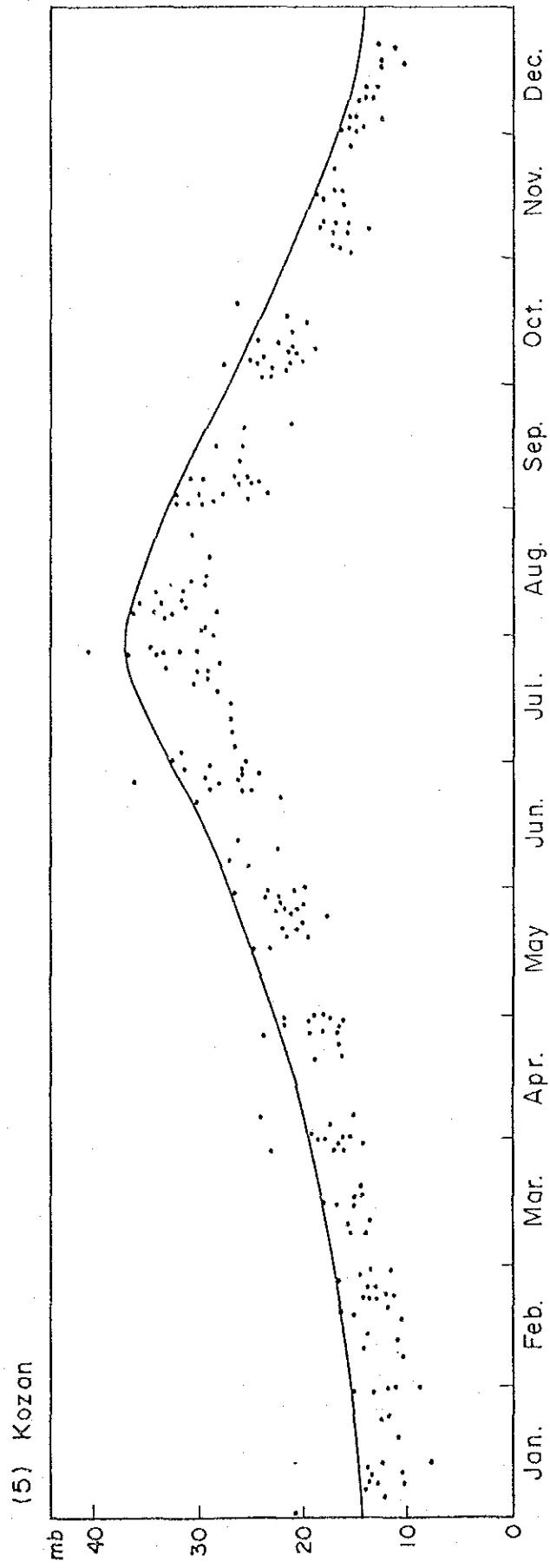




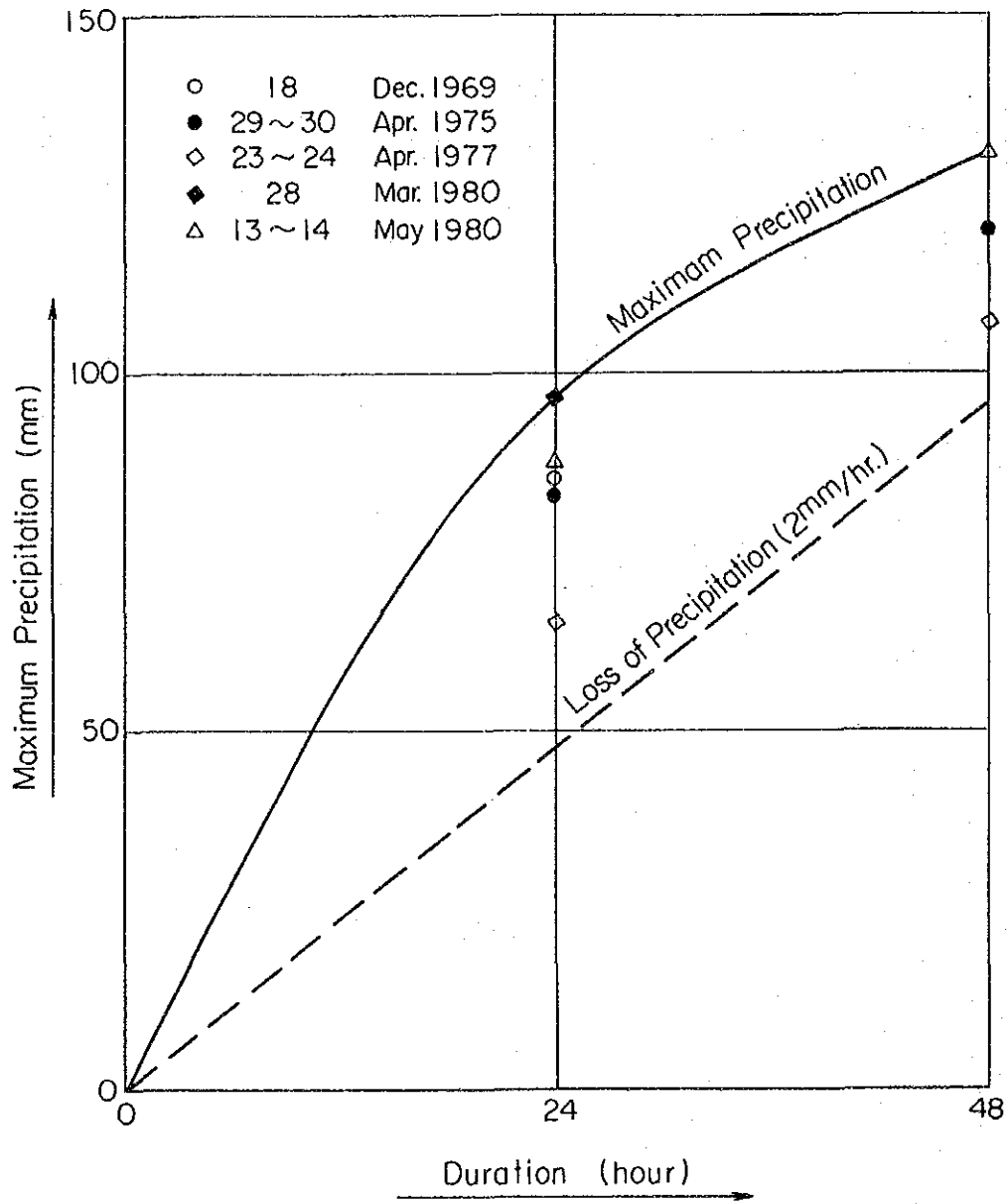
Table 6-29 Historical Storms Determined over the Zamanti River Basin and Their Maximization Results

Storm Date	Storm Duration (hour)	Average Precipitation (mm)	Real Precipitable Water: Ws (mm)	Maximum Precipitable Water: Wm (mm)	Wm/Ws	Maximum Precipitation (mm)
18 Dec. 1969	24	46.3	8.2	15.1	1.84	85.3/24 hr.
29-30 Apr. 1975	48	41.6	10.8	31.1	2.88	119.8/48 hr.
23-24 Apr. 1977	48	35.4	9.9	30.0	3.03	107.3/48 hr.
3 Jan. 1979	24	20.6	9.1	13.1	1.44	29.7/24 hr.
28 Mar. 1980	24	33.7	8.1	23.2	2.86	96.5/24 hr.
13-14 May 1980	48	49.3	13.0	34.5	2.65	130.6/48 hr.
22 May 1981	24	25.7	21.3	38.5	1.81	46.5/24 hr.
15 Oct. 1983	24	26.6	18.1	30.8	1.70	45.3/24 hr.

Table 6-30 Storm Maximization of the Historical Storm of 28th March, 1980

Item	Station		Vapour Pressure (mb)	Observed Dew-point Temperature (°C)	Dew-point Temperature at Sea-level (°C)	Precipitable Water above Sea-level (mm)	Correction for 1,600 m topographic barrier (mm)	Precipitable Water above 1,600 m level (mm)
	Name	Elevation						
Actual Values	Tomarza	1,400	6.8	1.5	9.4			
	Pinarbasi	1,470	7.6	3.0	11.2			
	Sariz	1,500	5.7	-0.9	7.9			
	Develi	1,180	5.4	-1.7	5.4			
	Kozan	150	12.5	10.3	11.0			
	Ave.				9.0	19.0	10.9	Ws = 8.1
Maximum Values	Tomarza	1,400	12.5	10.3	16.9			
	Pinarbasi	1,470	13.1	11.0	18.0			
	Sariz	1,500	13.4	11.3	18.3			
	Develi	1,180	13.2	11.1	16.7			
	Kozan	150	20.4	17.7	18.4			
	Ave.				17.7	42.8	19.6	Ws = 23.2
Maximization			Pac = 33.7 mm/24 hours		Pmax = Pac * $\frac{Wm}{Ws} = 33.7 * \frac{23.2}{8.1} = 96.5$ mm/24 hours			

Fig.6-24 DEPTH-DURATION CURVE OF MAXIMUM PRECIPITATION



### 6.6.3 Calculation of Probable Maximum Flood (PMF) at the Goktas Dam Site

#### (1) Calculation of Discharge from Probable Maximum Precipitation

##### (a) Effective Precipitation

The loss of precipitation in the Zamanti River basin was assumed to be uniformly 2 mm/hr with the relation between precipitation and runoff, and on deduction of this value from the depth-duration curve of PMP shown in Fig. 6-24, the maximum effective precipitation is calculated to be 48.5 mm/24 hr.

##### (b) Unit Hydrograph

Since hydrographs of past floods were not recorded at the No. 1806 Gauging Station downstream of the Goktas dam site, a unit graph for the site is prepared using the concept of Snyder's synthetic unit hydrograph. This unit hydrograph is prepared under the conditions of rainfall duration of 24 hours and rainfall intensity of 10 mm. The results are shown in Fig. 6-25.

##### (c) Probable Maximum Flood caused by PMP

The runoff hydrograph of the probable maximum flood caused by the PMP of effective rainfall intensity 48.5 mm/24 hr given in (a) above was determined by multiplying the 24 hr-10 mm unit hydrograph obtained in (b) by  $48.5 \text{ mm}/10 \text{ mm} = 4.85$ . This is shown in Fig. 6-26.

As a result, the peak discharge of probable maximum flood caused by PMP was calculated as  $2,720 \text{ m}^3/\text{s}$ .

#### (2) Calculation of Discharge from Probable Maximum Snowmelt (PMSM)

As mentioned in 6.6.1 (4), snowmelt is an important factor in floods in the basin of the Goktas Dam Site. For calculation of probable maximum snowmelt (PMSM) the method of multiplying cumulative air temperature (degree-days) by rate of snowmelt was used.

The maximum snowmelt ratio in the Zamanti River Basin was obtained as  $0.1 \text{ cm}/^\circ\text{C}\text{-day}$ , as a result of examination on relationship between

Fig.6-25 24hr-10mm Unit Hydrograph for the Goktas Damsite

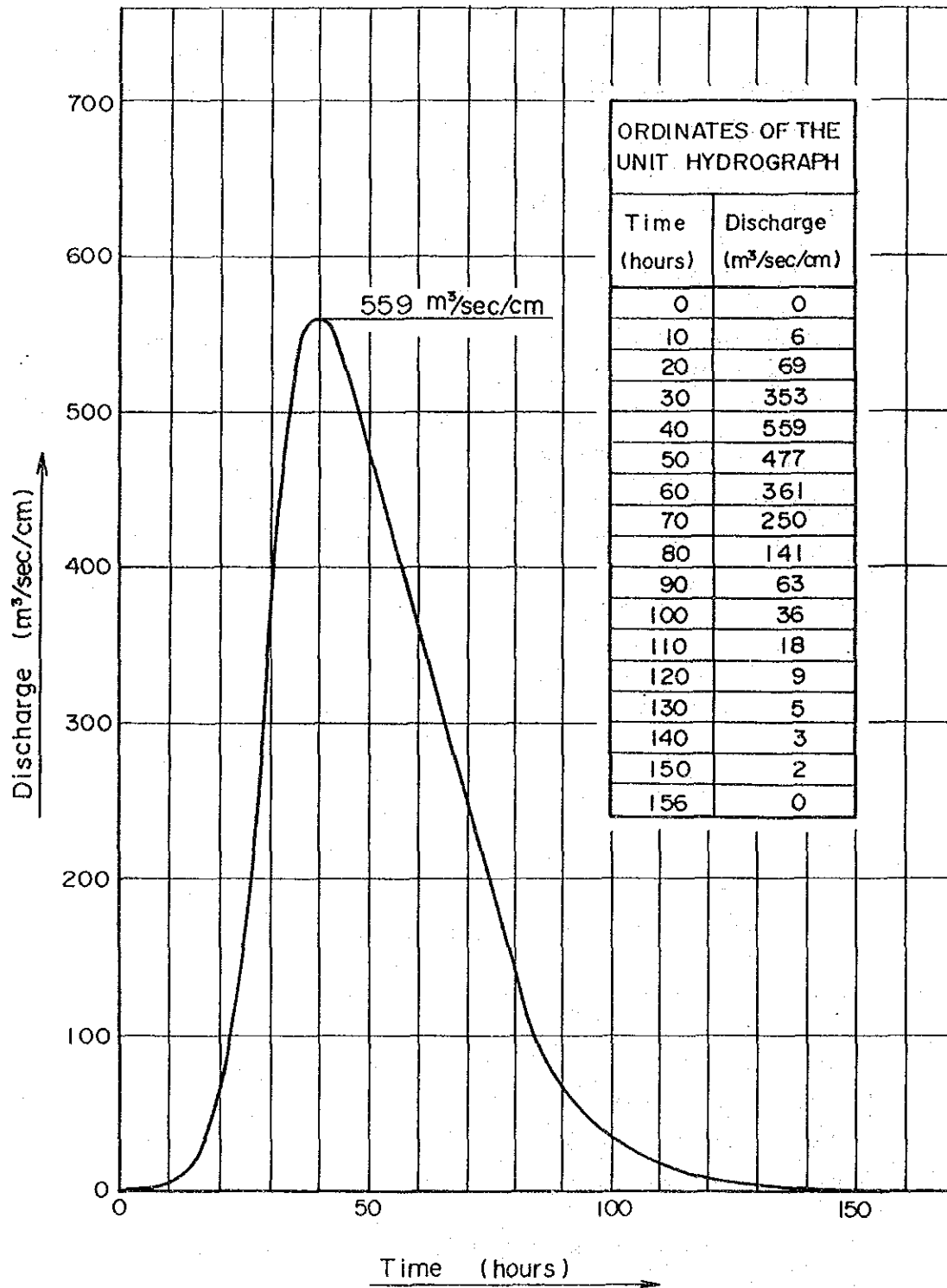
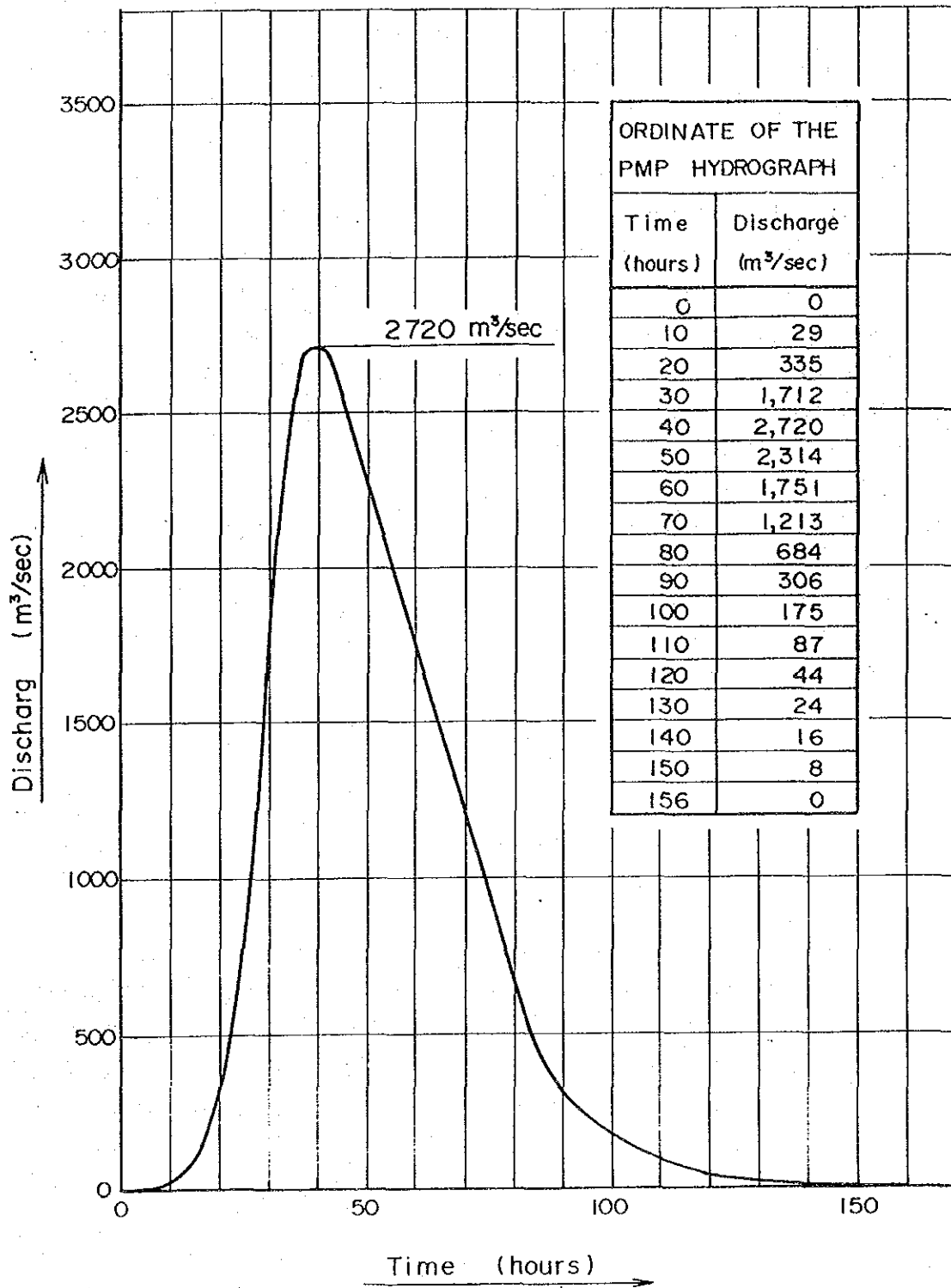


Fig 6-26 Probable Maximum Precipitation Runoff Hydrograph for the Goktas Damsite



discharge due to snowmelt and air temperature. The peak of outflow due to snowmelt in the Zamanti River Basin occurs during the period from March to April and the duration of this is a maximum of about 15 days. any snow cover seen in March or later is in areas higher than 1,500 m in elevation. On investigation of the area size of the Goktas Dam basin above EL. 1,500 m and the average elevation of such a zone, they were found to be approximately 5,900 km<sup>2</sup> and 1,800 m, respectively.

Further, the air temperatures at Pinarbasi in March-April were investigated considering the air temperature data of the Pinarbasi Meteorological Station (EL. 1,470 m) as being representative of the basin, and a model pattern of the maximum 15-day air temperature was prepared. This value was converted using the air temperature variation rate of 1°C/100 m on areas above the snowline of average elevation 1,800 m. The probable maximum snowmelt flood hydrograph at the Goktas dam site was obtained multiplying the maximum 15-day air temperature in the snow cover zone by the maximum snowmelt rate of 0.1 cm/°C-day and maximum snow cover area of 5,900 km<sup>2</sup>. This is shown in Table 6-31.

As a result, the peak discharge of probable maximum flood due to PMSM is calculated as 1,080 m<sup>3</sup>/s.

### (3) Probable Maximum Flood Discharge at the Goktas Dam Site

The base flow at the Goktas dam site is assumed as a maximum 100 m<sup>3</sup>/s on examination of the discharge data calculated for the 43-year period indicated in 6.2.4.

The hydrograph of probable maximum flood at the Goktas dam site is obtained by superimposing the hydrographs due to PMP and PMSM on the base flow of 100 m<sup>3</sup>/s. This is shown in Fig. 6-27. The peak discharge of PMF at the Goktas dam site is calculated to be 3,900 m<sup>3</sup>/s aggregating the peak discharges given in the table below.

Peak discharge of flood from PMP	2,720 m <sup>3</sup> /s
Peak discharge of flood from PMSM	1,080 m <sup>3</sup> /s
Maximum base flow	100 m <sup>3</sup> /s
Peak discharge of PMF	3,900 m <sup>3</sup> /s

(4) Probable Maximum Flood Peak Discharge at the Goktas Powerhouse Site

Following equation is get from the equation in 6.5.2 (2) on the relationship between the flood peak discharges at the Goktas Damsite and No. 1806 G.S.

$$FQ_{ps} = FQ_{1806} = \frac{1}{0.898} * FQ_{DAM}$$

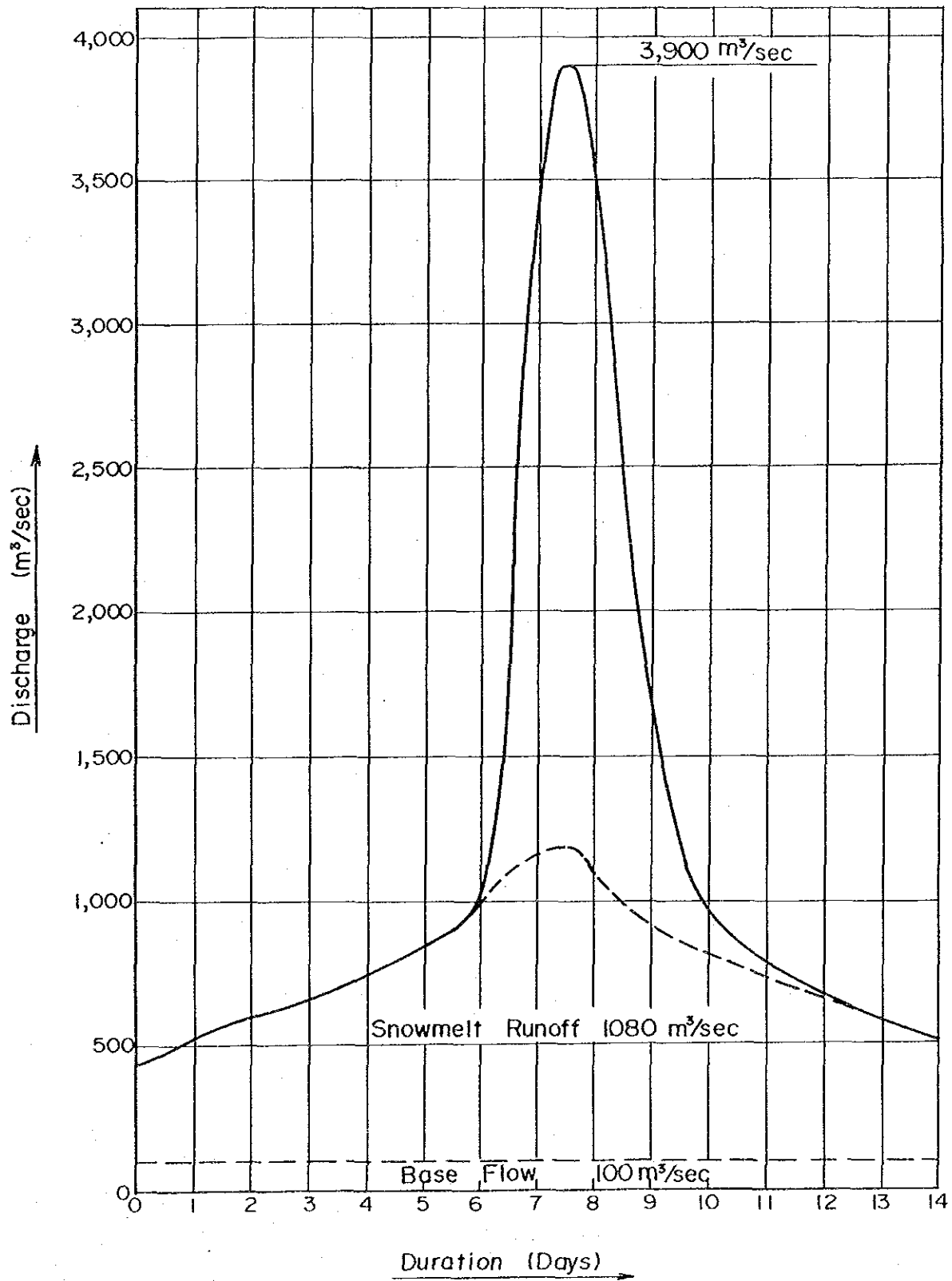
The probable maximum flood peak discharge of 4,400 m<sup>3</sup>/s at the Goktas Powerhouse site is calculated from the peak discharge of 3,900 m<sup>3</sup>/s at the Goktas Damsite using the above equation.



Table 6-31 Calculation of the Probable Maximum Snowmelt Runoff Hydrograph for the Goktas Damsite

Days	Maximum Continuous Daily Mean Temperature (°C)	Temperature at Average Elevation of Snow Cover (°C)	Temperature Arranged in Design Pattern (°C)	Daily Snowmelt with Maximum Snowmelt Ratio (cm)	Daily Snowmelt Volume (10 <sup>6</sup> m <sup>3</sup> )	Daily Snowmelt Discharge (m <sup>3</sup> /s)
1	19.1	15.8	5.5	0.55	32.45	376
2	17.9	14.6	6.8	0.68	40.12	464
3	15.4	12.1	7.6	0.76	44.84	519
4	14.8	11.5	7.6	0.76	44.84	519
5	14.3	11.0	10.1	1.01	59.59	690
6	13.4	10.1	11.5	1.15	67.85	785
7	13.2	9.9	14.6	1.46	86.14	997
8	10.9	7.6	15.8	1.58	93.22	1,079
9	10.9	7.6	12.1	1.21	71.39	826
10	10.9	7.6	11.0	1.10	64.90	751
11	10.9	7.6	9.9	0.99	58.41	676
12	10.1	6.8	7.6	0.76	44.84	519
13	8.8	5.5	7.6	0.76	44.84	519
14	8.8	5.5	5.5	0.55	32.45	376
15	8.8	5.5	5.5	0.55	32.45	376

Fig.6-27 Probable Maximum Flood Hydrograph for the Goktas Damsite



## **CHAPTER 7. GEOLOGY AND MATERIALS**

## CHAPTER 7. GEOLOGY AND MATERIALS

### CONTENTS

	<u>Page</u>
7.1 Introduction .....	7 - 1
7.2 Regional Geology .....	7 - 1
7.2.1 Topography .....	7 - 1
7.2.2 Geology .....	7 - 2
7.3 Outline of Investigations .....	7 - 9
7.3.1 Existing Data .....	7 - 9
7.3.2 Field Investigations .....	7 - 9
7.3.3 Geological Investigation Works .....	7 - 9
7.4 Geology of Reservoir Area .....	7 - 15
7.4.1 Topography .....	7 - 15
7.4.2 Geology .....	7 - 15
7.4.3 Hydrogeology .....	7 - 19
7.4.4 Considerations from the Viewpoint of Engineering Geology .....	7 - 19
7.5 Geology of Dam Site .....	7 - 27
7.5.1 Topography .....	7 - 27
7.5.2 Geology .....	7 - 27
7.5.3 Considerations from the Viewpoint of Engineering Geology .....	7 - 30

	<u>Page</u>
7.6 Geologies of Other Structure Sites .....	7 - 49
7.6.1 Intake Site .....	7 - 49
7.6.2 Headrace Tunnel Route .....	7 - 49
7.6.3 Surge Tank, Penstock, and Powerhouse Sites .....	7 - 53
7.7 In-situ Rock Tests at Dam Site .....	7 - 65
7.7.1 Introduction .....	7 - 65
7.7.2 Plate Bearing Test .....	7 - 65
7.7.3 Block Shear Test .....	7 - 68
7.7.4 Results of Tests and Evaluations .....	7 - 70
7.8 Geophysical Prospecting of Powerhouse Site .....	7 - 78
7.8.1 Introduction .....	7 - 78
7.8.2 Selection of Prospecting Location .....	7 - 78
7.8.3 Prospecting Method .....	7 - 82
7.8.4 Results and Evaluations .....	7 - 84
7.9 Construction Materials .....	7 - 99
7.9.1 Investigations and Tests .....	7 - 99
7.9.2 Concrete Aggregates .....	7 - 100

## List of Figures

- Fig. 7-1 Regional Geological Plan
- Fig. 7-2 Geological Map of Reservoir Area
- Fig. 7-3 Geological Plan of Dam Site
- Fig. 7-4 Geological Section of Dam Site
- Fig. 7-5 Point and Contour Diagrams of All Measured Cracks in Adits
- Fig. 7-6 Point and Contour Diagrams of Serpentinization Cracks in Adits
- Fig. 7-7 Rock Evaluation
- Fig. 7-8 Location Map of Proposed Dam Axes
- Fig. 7-9 Geological Plan and Profile of Headrace Tunnel Route
- Fig. 7-10 Geological Plan of Surge Tank, Penstock and Powerplant Sites
- Fig. 7-11 Geological Profile of Surge Tank, Penstock and Powerplant Sites
- Fig. 7-12 Relation Between Rock Classification and Deformation or Shear Strength
- Fig. 7-13 Results of Block Shear Test and Estimated Shear Strength
- Fig. 7-14 Location Map of Seismic Prospecting Line
- Fig. 7-15 Diagram of Seismic Prospecting Method
- Fig. 7-16 PS-1 Time-Distance Plot and Seismic Profile
- Fig. 7-17 PS-2 Time-Distance Plot and Seismic Profile
- Fig. 7-18 PS-3 Time-Distance Plot and Seismic Profile
- Fig. 7-19 PS-1, PS-2, PS-3, Reanalysis Profiles
- Fig. 7-20 Location Map of Quarry and Borrow Area

## List of Tables

Table 7-1	General Stratigraphic Section of Surveying Area
Table 7-2	Reference Data
Table 7-3	List of Geological Investigations
Table 7-4	Stratigraphic Section of Reservoir Area
Table 7-5	Chemical Analysis of Limestone in Reservoir Area
Table 7-6	Laboratory Test Results of Drilled Cores at Dam Site
Table 7-7	Standard of Rock Classification
Table 7-8	Laboratory Test Results of Drilled Cores at Headrace Tunnel Route
Table 7-9	Laboratory Test Results of Drilled Cores at Power Plant Site
Table 7-10	Location of Plate Bearing Tests
Table 7-11	Equipment and Device for Plate Bearing Test
Table 7-12	Location of Block Shear Test
Table 7-13	Equipment and Device for Block Shear Test
Table 7-14	Results of Plate Bearing Test
Table 7-15	Results of Block Shear Test
Table 7-16	List of Location of Seismic Prospecting Line and Drillhole
Table 7-17	Quantity of Seismic Prospecting
Table 7-18	List of Seismic Prospecting Instrument
Table 7-19	Classification of Velocity Layer
Table 7-20	PS-1 Seismic Analysis and Drilling Data
Table 7-21	PS-2 Seismic Analysis and Drilling Data
Table 7-22	PS-3 Seismic Analysis and Drilling Data
Table 7-23	Quantity of Laboratory Tests for Construction Materials
Table 7-24	Laboratory Test Results for Concrete Aggregate (Quarry Site)
Table 7-25	Laboratory Test Results for Concrete Aggregate (RD Site)

## CHAPTER 7. GEOLOGY AND MATERIALS

### 7.1. Introduction

Geological investigation works concerning the Goktas Hydroelectric Power Development Project were started by the DSI in 1987, and the geological investigation works of the items and quantities given in Table 7-3 were completed by November 1988. During this time, survey teams from JICA carried out field geological investigations on two occasions (first: November 14 to December 28, 1987; second: September 6 to November 4, 1988).

This chapter describes the geological, hydrogeological, and engineering geological conditions of the project area, dam site, and major structure sites disclosed through the field investigations made by the JICA Survey Team, and the various investigation works and results of numerous tests carried out by the DSI.

### 7.2. Regional Geology

#### 7.2.1 Topography

The project area of the Goktas Project is located at the downstream-most stretch of the Zamanti River, one of the two principal tributaries of the Seyhan River which runs through the southern part of Turkey. The Seyhan River, rising from the mountainland of Central Anatolia and flowing south to empty into the Mediterranean Sea, is one of the largest rivers of Turkey with a length of 506 km and catchment area of 20,730 km<sup>2</sup>. The upstream part of the Seyhan River consists of the two large tributaries of the Zamanti and Goksu.

A general look at the topography in the basin of the Zamanti-Seyhan river system shows the following divisions from the upstream to the downstream stretches. Namely, they are the fountainhead area of elevation around 2,000 m belonging to the Central Anatolian Plateau (hereinafter called "Fountainhead Area"), the Toros Mountain Range area where rugged mountains of elevation from 2,000 to 3,000 m run in a southwest-northeast direction (hereinafter called "Toros Mountain Range Area"), and a hill-and-plain area of elevation 300 m



and under centered at Adana (hereinafter called "Hill-and-Plain Area).

The Goktas Project area is situated where the Zamanti River cuts across the Toros Mountain Range, and because of this, the project area is featured by topography at a stage of maturity having rugged mountains of elevation 2,000 m and deeply eroded valleys. The greater part of the Zamanti River is of gorge form and the river gradient is steep, averaging 1/100.

## 7.2.2 Geology

The geologic province of Turkey can be classified according to four east-west band-like tectonic provinces of the Pontids, Anatolids, Taurids, and Border Folds. The Zamanti River Basin is situated in the Taurids tectonic province among these, which stretches from the Mediterranean Sea coast to the eastern part of Turkey.

### (1) Geology of the River Basin

The geology of the Zamanti-Seyhan Basin, as shown in Fig. 7-1, mainly consists of Paleozoic sedimentary rocks (sandstone, shale, dolomite, limestone, etc.), Mesozoic carbonate rocks, similarly Mesozoic ultrabasic to basic rocks (ophiolite), Paleogene volcanic rocks (basalt, andesite, tuff, etc.), and Neogene sedimentary rocks (sandstone, mudstone, marl, etc.).

The distributions of these rocks are closely related to topography, and of the beforementioned topographic classifications, the Fountainhead Area is mainly composed of Paleogene volcanic rocks, and the Hill-and-Plain Area of Neogene sedimentary rocks. And the geology comprising the Toros Mountain Range Area is composed of Paleozoic sedimentary rocks, Mesozoic carbonate rocks, and ophiolite.

These pre-Tertiary rocks comprising the Toros Mountain Range generally extend in the southwest-northeast direction and the strikes of bedding are also southwest-northeast. Faults of comparatively great lengths in the river basin are seen predominantly

in the Paleozoic sedimentary rocks and the directions of these faults are southwest-northeast to south-southwest-north-northeast.

Tectonic lines or major faults delineating geologic structures as seen from the standpoint of entire Turkey are not distributed in the basin. Outside the basin, the Eceemis Fault (a fault extending south-southwest to north-northeast from the vicinity of Kayseri in the central part of Turkey to Mersin facing the Mediterranean Sea) and the East Anatolian Fault (a fault extending southwest-northeast from west of Lake Van toward Antakya near the border with Syria) are located comparatively close to the basin. The former is situated approximately 50 km to the west of the Zamanti River, and the latter approximately 150 km to the east.

## (2) Geology of Project Site

The geology around the site of the Goktas Project mainly consists of Paleozoic sedimentary rocks such as sandstone and shale with interbedding of limestone, Mesozoic limestone, and also Mesozoic ophiolite. The general stratigraphic section of the project site is shown in Table 7-1.

In general, the Paleozoic sedimentary rocks are distributed at the southeast side of the project area, that is, the downstream side of the Zamanti River, while at the northeast side, or the upstream side, Mesozoic limestone is distributed along with ophiolite. The strikes of strata are southwest-northeast to south-southwest-north-northeast, and faults also show strikes of the same directions in most cases. The relation between the Mesozoic limestone and the ophiolite is considered to be that of a nappe with the ophiolite riding on top of limestone.

The distributions of the various rocks and the geologies of basement rocks of projected structures are approximately as follows:

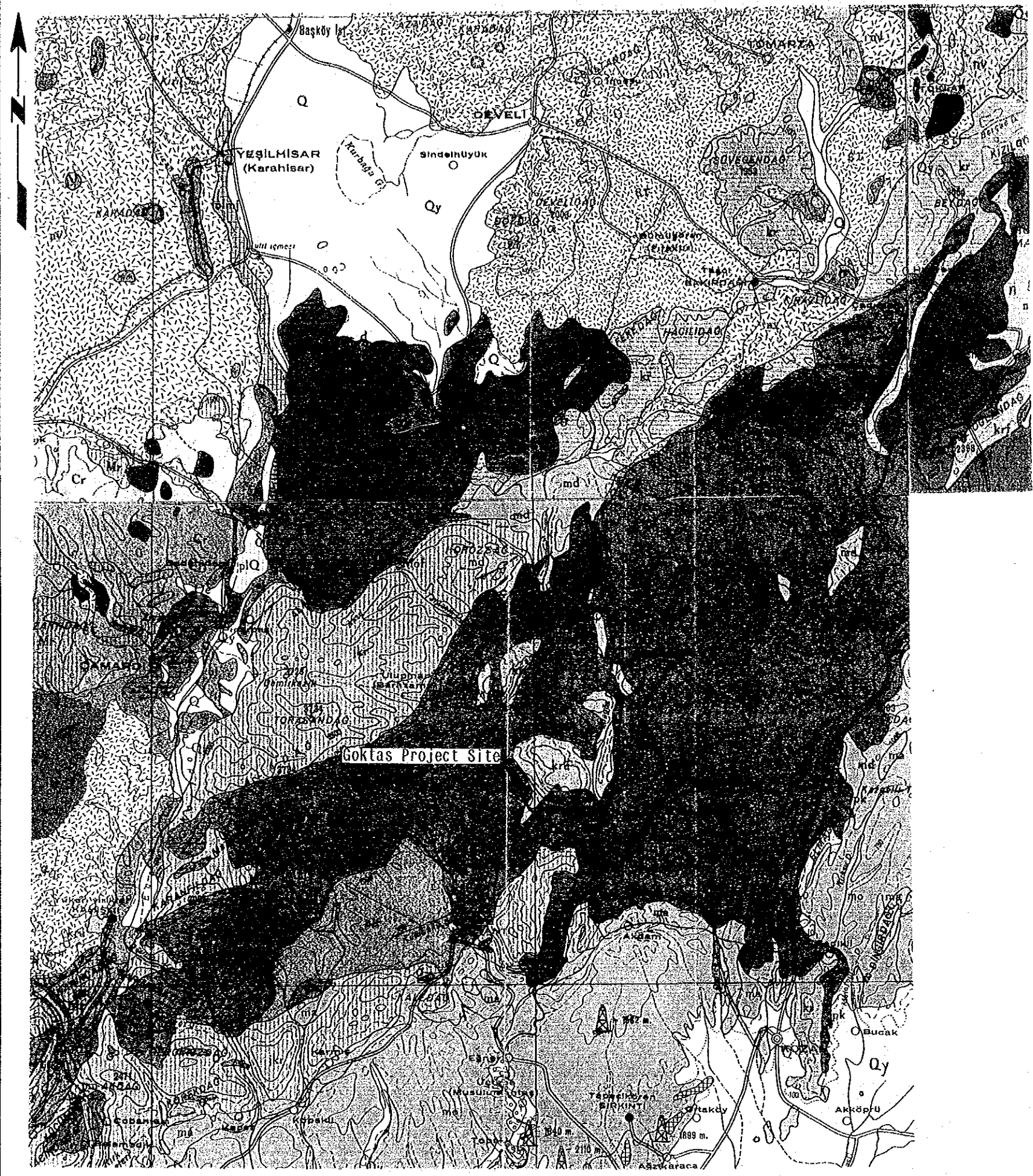
Reservoir end vicinity: Mesozoic limestone  
Reservoir, dam : Mesozoic ophiolite  
Headrace tunnel : Mesozoic ophiolite and limestone,  
Paleozoic limestone, sandstone, shale  
Powerhouse : Paleozoic sandstone, shale, limestone

Table 7-1 General Stratigraphic Section of Surveying Area

Upper Systems		System	Series	Symbol	Lithology
CENOZOIC	QUATERNARY	HOLOCENE	al		ALLUVIUM Large blocky, main pieces is Peridotite with few Limestone and Quartzite.
			ym		SLOPE MATERIAL Blocks are Limestone, Quartzite, and Ophiolite with fine material.
			Trv		TRAVERTINE Soft and porous
		PLEISTOCENE	Tr		TERRACE CONGLOMERATE Polygenetic gravels, weak cemented, cement is CaCO <sub>3</sub> UNCONFORMITY
MESOZOIC	JURASSIC/CRETACEOUS	UPPER CRETACEOUS	Of		OPHIOLITE It is Peridotite at damsite. Light-dark green coloured. OVERTHRUST
			Kp		SANDSTONE - SILTSTONE - SHALE Yellow-green coloured, thin and medium thick bedded. Weak strength. UNCONFORMITY
		Jkr		LIMESTONE Dirty white coloured, interbedded with dolomite. Medium thick bedded. Very high strength. UNCONFORMITY	
PALAEOZOIC	CARBONIFEROUS/PERMIAN		Pk		LIMESTONE - CLAYEY LIMESTONE - BITUMINOUS SHALE Dark gray, black coloured, with some dolomitic layers, medium thick bedded. UNCONFORMITY
	DEVONIAN		D		LIMESTONE - DOLOMITIC LIMESTONE - SHALE - SANDSTONE - QUARTZITE This unites are interbedded. Shale layers are thin bedded and weak strength. Other layers are medium thick bedded and good strength. UNCONFORMITY
	ORDOVICIAN		O		SHALE - SILTSTONE Thin bedded, partly flaky. Siltstone is predominant at upper layers.
	CAMBRIAN	UPPER	Eo		LIMESTONE Dark gray, black coloured sound and thick bedded. UNCONFORMITY
		LOWER/MIDDLE	Ea		SANDSTONE - SILTSTONE - CLAYSTONE - QUARTZITE - LIMESTONE Horizontal and vertical transition to each unites.



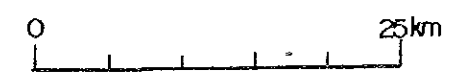




LEGEND

- |     |  |  |
|-----|--|--|
| Q   | KUATERNER, KARASAL, AYRILMAMIŞ<br>QUATERNARY, CONTINENTAL, UNDIFFERENTIATED                    | DİORİT, GABRO, DIABAZ<br>DIORITE, GABBRO, DIABASE                        |
| Qy  | HOLOSEN, YENİ ALÜVYON<br>HOLOCENE, RECENT  | PERİDOTİT, PİROKSENİT, HARZBURGİT<br>PERIDOTITE, PYROXENITE, HARZBURGITE |
| pQ  | PLİO - KUATERNER<br>PLIG - QUATERNARY  | SERPANTİN<br>SERPENTINE  |
| N   | NEOJEN, KARASAL, AYRILMAMIŞ<br>NEOGENE, CONTINENTAL, UNDIFFERENTIATED                          | ANDEZİT, SPİLİT, PORFİRİT<br>ANDESITE, SPILITE, PORPHYRITE               |
| Nv  | NEOJEN, VOLKANİK FASİES<br>NEOGENE, VOLCANIC FACIES  | BAZALT, DOLERİT<br>BASALT, DOLERITE                                      |
| M   | MİOSEN, DENİZEL, AYRILMAMIŞ<br>MIOCENE, MARINE, UNDIFFERENTIATED                               | VOLKANİK TÜF, AGLOMERA, BRES<br>VOLCANIC TUFF, AGGLOMERATE, BRECCIA      |
| Mo  | ORTA MİOSEN<br>MIDDLE MIOCENE  | TRAVERTEN<br>TRAVERTINE  |
| Ml  | ALT MİOSEN<br>LOWER MIOCENE  | SEKİ, (TARACA)<br>TERRACE  |
| O   | OLİGO - MİOSEN, DENİZEL<br>OLIGO - MIOCENE, MARINE   | KRATER<br>CRATER   |
| Og  | OLİGOSEN, KARASAL<br>OLIGOCENE, CONTINENTAL  | FORMASYON SINIRI<br>FORMATION BOUNDARY                                   |
| Ofl | OLİGOSEN, FLİŞ<br>OLIGOCENE, FLYSCH  | MUHTEMEL FORMASYON SINIRI<br>ESTIMATED BOUNDARY                          |
| E   | EÖSEN, AYRILMAMIŞ<br>EOCENE, UNDIFFERENTIATED  | ŞARİYAL, BİNDİRME, FAY<br>OVERTHRUST, UPTHRUST, FAULT                    |
| Ef  | EÖSEN, FLİŞ<br>EOCENE, FLYSCH  | MUHTEMEL ŞARİYAL, BİNDİRME, FAY<br>PROBABLE OVERTHRUST, UPTHRUST, FAULT  |
| Em  | ORTA EÖSEN, LÖTESİEN<br>MIDDLE EOCENE, LUTETIAN  | PETROL ARAMA KUYULARI<br>OIL EXPLORATION WELLS                           |
| M   | MESOZOİK (OFİOLİTLİ SERİ), EKSERİYLA KRETASE<br>MESOZOIC (OPHOLITIC SERIES), MAINLY CRETACEOUS | KROM<br>CHROMITE   |
| K   | KRETASE, AYRILMAMIŞ<br>CRETACEOUS, UNDIFFERENTIATED  | DEMİR<br>IRON  |
| Kü  | ÜST KRETASE<br>UPPER CRETACEOUS  |  |
| J   | JURA - KRETASE<br>JURASSIC - CRETACEOUS  |  |
| P   | PERMO - KARBONİFER<br>PERMO - CARBONIFEROUS  |  |
| D   | DEVONİYEN<br>DEVONIAN  |  |
| S   | SİLÜRİYEN<br>SILURIAN  |  |
| M   | METAMORFİK SERİ, AYRILMAMIŞ<br>METAMORPHIC SERIES, UNDIFFERENTIATED                            |  |
| M   | MERMER, KRİSTALİZE KALKER VE DOLOMİT<br>MARBLE, CRYSTALLINE LIMESTONE AND DOLOMITE             |  |
| G   | GRANİT, GRANODİORİT, KUARSIZ DİORİT<br>GRANITE, GRANODIORITE, QUARTZ - DIORITE                 |  |

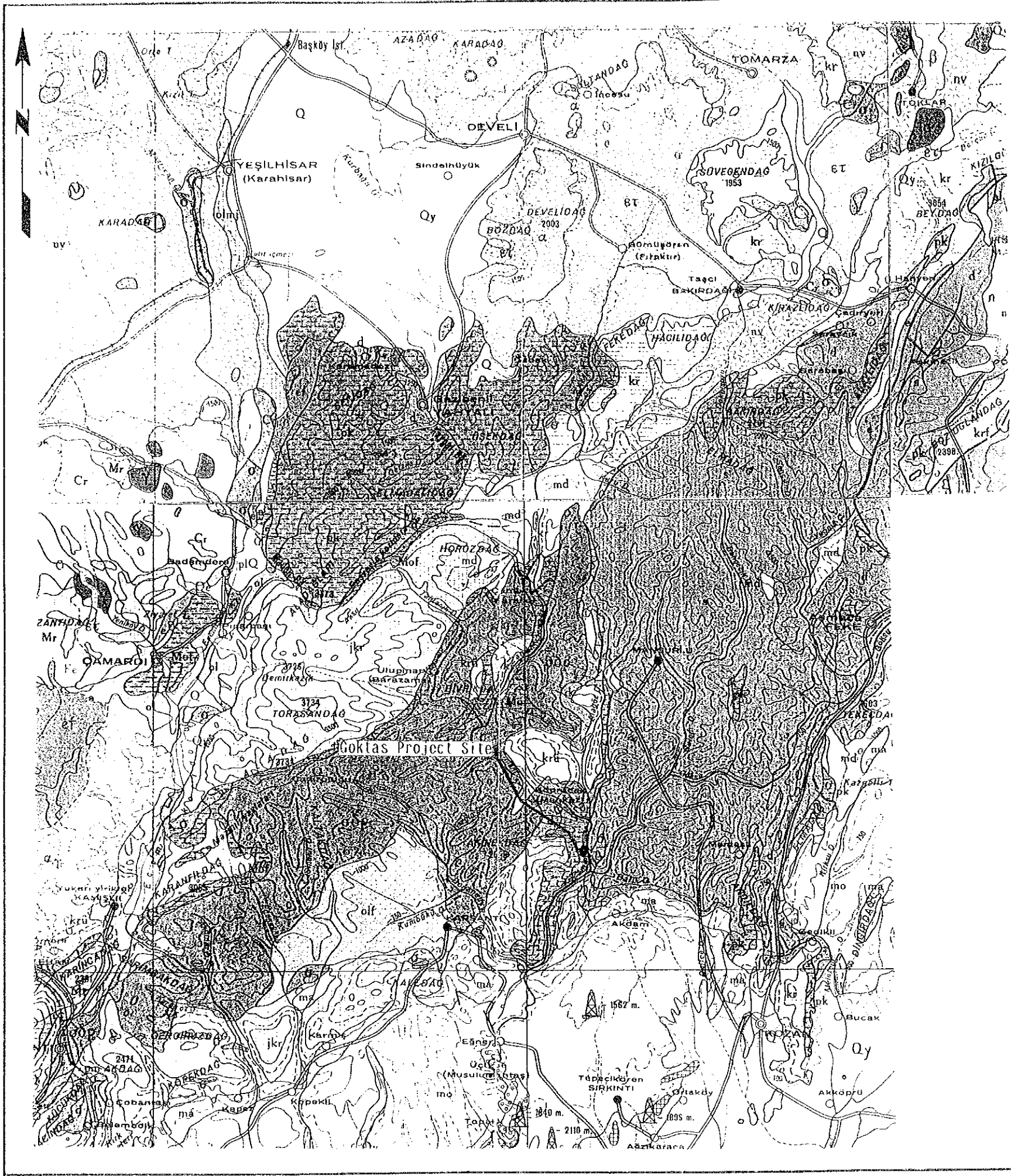
Note; This map is compiled from  
GEOLOGICAL MAP OF  
TURKEY "ADANA", "KAYSERİ"  
and "SIVAS" (SCALE 1/500,000)  
by MTA ANKARA - TURKEY



ZAMANTI GÖKTAŞ HYDROELECTRIC  
POWER DEVELOPMENT PROJECT

REGIONAL GEOLOGICAL  
PLAN

Fig. 7 - 1



LEGEND

- Q KUATERNER KARASAL AYRILMAMIS  
QUATERNARY CONTINENTAL UNDIFFERENTIATED
- Qy HOLOSEN, KENI ALLUVYON  
HOLOCENE, NEW ALLUVIUM
- plQ PLIO KUATERNER  
PLIOCENE QUATERNARY
- n NEOJEN KARASAL AYRILMAMIS  
NEOGEN CONTINENTAL UNDIFFERENTIATED
- nv NEOJEN VOLKANIK FASIES  
NEOGEN VOLCANIC FACIES
- md MIOSEN DENIZEL AYRILMAMIS  
MIOCENE MARINE UNDIFFERENTIATED
- mo ORTA MIOSEN  
MIDDLE MIOCENE
- ma ALT MIOSEN  
LOWER MIOCENE
- ulm OLGUN MIOSEN DENIZEL  
UPPER MIOCENE MARINE
- ul OLGUN MIOSEN KARASAL  
UPPER MIOCENE CONTINENTAL
- oll OLGUN MIOSEN FLIS  
UPPER MIOCENE FLINT
- e Eosen AYRILMAMIS  
Eocene UNDIFFERENTIATED
- el Eosen FLIS  
Eocene FLINT
- l ORTA Eosen LUTESIEN  
MIDDLE Eocene LUTETIAN
- MoF MESOZIK OTOJENELE AFRIKASIA KRETASE  
MESOZOIC AUTOGENEOUS AFRICAN CRETACEOUS
- kr KRETASE AYRILMAMIS  
CRETACEOUS UNDIFFERENTIATED
- krü ÜST KRETASE  
UPPER CRETACEOUS
- jkr JURA KRETASE  
JURASSIC CRETACEOUS
- k PERMO KARBONIFER  
PERMIAN CARBONIFEROUS
- d DEVÖVEN  
DEVONIAN
- s SİLURİYEN  
SILURIAN
- Cr METAMORFİK SERP AYRILMAMIS  
METAMORPHIC SERPENTINE UNDIFFERENTIATED
- Mr MERMER KRISTALLE KALKEN VE DOLOMIT  
MARMAR MARBLES, Limestones and Dolomites
- G GRANİT GRANODIORİT KUARSİT DORİT  
GRANITE GRANODIORITE QUARTZITE DIORITE
- DORT GABRO İNHAZ  
FOUR GRANITE MASSIF
- PERİODİT BİROSENİ, HAZİRUR  
PERIODITE BIROSENI, HAZIRUR
- SERPANTİN  
SERPENTINE
- α ANFİZİT, SİLİT, PORFİRİT  
ANFIZITE, SILITE, PORPHYRITE
- β BAZALT, DOLOMIT  
BASALT, DOLOMITE
- BT LÖLÜMÜZLÜ TÜF, AGLOMERAT, BRES  
LOLUMUZLU TUF, AGLOMERATE, BRECCIA
- TRAVERTİN  
TRAVERTINE
- SERİ KARACAI  
SERI KARACAI
- HASEL  
HASSEL
- FORMASYON SINIRI  
FORMATION BOUNDARY
- MÜTEVELLİ FORMASYON SINIRI  
CONFORMITY BOUNDARY
- SARIYAZI BİNDİRME FAYI  
SARIZI BOUNDING FAULT
- MÜTEVELLİ SARIYAZI BİNDİRME FAYI  
CONFORMITY SARIZI BOUNDING FAULT
- PETROL ARAMA AYKULARI  
PETROLEUM PROSPECTS
- KIRMIZI  
RED
- DEMİR  
IRON

Note: This map is compiled from  
GEOLOGICAL MAP OF  
TURKEY "ADANA", "KAYSERİ"  
and "SIVAS" (SCALE 1/500,000)  
by MTA ANKARA - TURKEY



ZAMANTI GÖKTAŞ HYDROELECTRIC  
POWER DEVELOPMENT PROJECT

REGIONAL GEOLOGICAL  
PLAN

Fig. 7 - 1





- Q
- Q<sub>1</sub>
- Q<sub>2</sub>
- Q<sub>3</sub>
- Q<sub>4</sub>
- Q<sub>5</sub>
- Q<sub>6</sub>
- Q<sub>7</sub>
- Q<sub>8</sub>
- Q<sub>9</sub>
- Q<sub>10</sub>
- Q<sub>11</sub>
- Q<sub>12</sub>
- Q<sub>13</sub>
- Q<sub>14</sub>
- Q<sub>15</sub>
- Q<sub>16</sub>
- Q<sub>17</sub>
- Q<sub>18</sub>
- Q<sub>19</sub>
- Q<sub>20</sub>
- Q<sub>21</sub>
- Q<sub>22</sub>
- Q<sub>23</sub>
- Q<sub>24</sub>
- Q<sub>25</sub>
- Q<sub>26</sub>
- Q<sub>27</sub>
- Q<sub>28</sub>
- Q<sub>29</sub>
- Q<sub>30</sub>
- Q<sub>31</sub>
- Q<sub>32</sub>
- Q<sub>33</sub>
- Q<sub>34</sub>
- Q<sub>35</sub>
- Q<sub>36</sub>
- Q<sub>37</sub>
- Q<sub>38</sub>
- Q<sub>39</sub>
- Q<sub>40</sub>
- Q<sub>41</sub>
- Q<sub>42</sub>
- Q<sub>43</sub>
- Q<sub>44</sub>
- Q<sub>45</sub>
- Q<sub>46</sub>
- Q<sub>47</sub>
- Q<sub>48</sub>
- Q<sub>49</sub>
- Q<sub>50</sub>
- Q<sub>51</sub>
- Q<sub>52</sub>
- Q<sub>53</sub>
- Q<sub>54</sub>
- Q<sub>55</sub>
- Q<sub>56</sub>
- Q<sub>57</sub>
- Q<sub>58</sub>
- Q<sub>59</sub>
- Q<sub>60</sub>
- Q<sub>61</sub>
- Q<sub>62</sub>
- Q<sub>63</sub>
- Q<sub>64</sub>
- Q<sub>65</sub>
- Q<sub>66</sub>
- Q<sub>67</sub>
- Q<sub>68</sub>
- Q<sub>69</sub>
- Q<sub>70</sub>
- Q<sub>71</sub>
- Q<sub>72</sub>
- Q<sub>73</sub>
- Q<sub>74</sub>
- Q<sub>75</sub>
- Q<sub>76</sub>
- Q<sub>77</sub>
- Q<sub>78</sub>
- Q<sub>79</sub>
- Q<sub>80</sub>
- Q<sub>81</sub>
- Q<sub>82</sub>
- Q<sub>83</sub>
- Q<sub>84</sub>
- Q<sub>85</sub>
- Q<sub>86</sub>
- Q<sub>87</sub>
- Q<sub>88</sub>
- Q<sub>89</sub>
- Q<sub>90</sub>
- Q<sub>91</sub>
- Q<sub>92</sub>
- Q<sub>93</sub>
- Q<sub>94</sub>
- Q<sub>95</sub>
- Q<sub>96</sub>
- Q<sub>97</sub>
- Q<sub>98</sub>
- Q<sub>99</sub>
- Q<sub>100</sub>

LEGEND

- Q
- P
- A
- E
- N
- UV
- MD
- MO
- MA
- IR
- UD
- OF
- F
- EF
- CF
- MOF
- K
- KR
- PK
- D
- A
- Cr
- Mr
- Y

NOTE: This map is prepared by the Ministry of Energy, Water and Coal, Turkey, Ankara, 1987, and "Scale" 1:500,000, by MTA, Ankara, 1987.

ZAMANTI GOKTAS HYDROELECTRIC POWER DEVELOPMENT PROJECT  
REGIONAL GEOLOGICAL PLAN



### 7.3 Outline of Investigations

#### 7.3.1 Existing Data

The geological data used as references in writing this Report are as listed in Table 7-2.

#### 7.3.2 Field Investigations

The JICA Survey Team carried out geological investigations during the two periods below.

First : November 14 to December 28, 1987

Second: September 6 to November 4, 1988

The contents of the investigations made by the JICA Survey Team during the respective field investigation periods were as follows:

- First : - Site reconnaissance  
- Data collection and analyses thereof
- Second: - Surface geological mapping  
- Geological observation of drilled cores and adits  
- Supportive supervision of in-situ tests and review of test results  
- Confirmation of seismic prospecting and review of prospecting results  
- Data collection

#### 7.3.3 Geological Investigation Works

The outline of the geological investigation works carried out in the Goktras project area is as indicated below. Details are given in Table 7-3.

Drilling (including permeability tests)	12 holes	Total 1,091 m
Exploratory adit	2 adits	Total 131.5 m
Plate bearing test		Total 7 points
Block shear test		Total 8 blocks
Seismic prospecting	3 profiles	Total 865 m
Drilled core test		Total 20 samples
Material test	7 sites	Total 95 samples

Table 7-2 Reference Data

	Items	Notes
1	Lower Seyhan Basin Master Plan Report	DSI, Aug. 1980
2	Yukari Seyhan Projeleri Master Plan, Muhendislik Jeolojisi Raporu	DSI, 1983
3	Yukari Seyhan Havzasi Master Plan Raporu	DSI, Sep. 1984
4	Geological Map of Turkey (1/500,000) Adana	MTA, 1962
5	Geological Map of Turkey (1/500,000) Kayseri	MTA, 1961
6	Geological Map of Turkey (1/500,000) Sivas	MTA, 1961
7	Geological Map of the Kozan-J20 Quadrangle (1/100,000)	MTA, 1987
8	Geological Map of the Kozan-J21 Quadrangle (1/100,000)	MTA, 1988
9	Yukari Seyhan Projesi, Goktas Baraji Gol Alanı Muhendislik Jeolojisi Planlama Raporu	DSI, Aug. 1988
10	Geological Map of Goktas Dam Site	DSI, Dec. 1988
11	Geological Map of Goktas Headrace Tunnel Route	DSI, Dec. 1988
12	Geological Map of Goktas Power Plant Site	DSI, Dec. 1988
13	Logs of Drillholes and Drilling Data	DSI, Nov. 1988
14	Permeability Test Data	DSI, Nov. 1988
15	Laboratory Test Data and Microscopic Observation Data of Drilling Cores	DSI, Nov. 1988
16	Laboratory Test Data for Construction Materials	DSI, 1988
17	Plate Bearing and Block Shear Test Data	DSI, 1988
18	Goktas Baraji Hes Yeri Ve Cebri Boru Guzergahi Sismik Refraksiyon Etudu	DSI, 1988





Table 7-3 List of Geological Investigations

[Drillhole]

Hole No.	Coordinate		Elevation(m)	Length(m)	Direction	Dip	Permeability Test(Stage)
	X	Y					
SK-1	-	-	510	100.0	-	90°	38
SK-2	452,695.19	4,178,050.45	510.834	70.0	-	90°	26
SK-3	452,559.74	4,177,956.03	607.609	100.0	-	90°	50
SK-4	452,560.15	4,177,955.30	607.222	80.0	S25E	45°	40
SK-5	452,534.29	4,178,057.82	517.561	100.0	S40E	55°	31
SK-6	452,510.97	4,178,097.07	542.365	90.0	-	90°	44
SK-7	452,439.67	4,178,108.32	603.687	80.0	N25W	60°	40
TB-1	455,751.98	4,172,232.91	631.375	90.0	-	90°	44
TB-2	460,825.80	4,168,653.59	740.076	190.0	-	90°	40
PB-1	462,758.59	4,166,135.85	391.912	71.0	-	90°	34
PB-2	462,565.39	4,166,145.90	521.353	70.0	-	90°	35
SSK-1	453,591.59	4,177,144.65	520.518	50.0	-	90°	7
Total 12 Holes				1091.0			429

[In-situ Rock Test]

Adit No.	Plate bearing test		Block shear test	
	Test No.	Location(m)	Test No.	Location(m)
DA-1	P-1	20.0	BS-1	15.4
DA-1	P-2	40.5	BS-2	17.4
DA-1	P-3	(B.)2.1	BS-3	18.6
DA-1	P-4	(B.)4.0	BS-4	19.9
DA-2	P-1	16.3	BS-1	10.8
DA-2	P-2	19.0	BS-2	12.0
DA-2	P-3	(B.)5.8	BS-3	13.5
			BS-4	15.7
Total	7 Tests		8 Tests	

[Adit]

Adit No.	Coordinate		Elevation(m)	Length(m)	Branch Length(m)	Direction
	X	Y				
DA-1	452,583.35	4,178,021.05	513.611	68.0	10.0	S20E
DA-2	-	-	545.382	63.5	10.0	N20W-N30W
Total 2 Adits				131.5	20.0	

[Seismic Prospecting]

Line No.	Coordinate		Length(m)
	Beginning point	Ending point	
PS-1	X. 462,556.3	X. 462,229.0	340m
	Y.4,166,116.2	Y.4,166,211.7	
PS-2	X. 462,395.2	X. 462,550.1	370m
	Y.4,166,410.5	Y.4,166,075.8	
PS-3	X. 462,767.0	X. 462,737.5	155m
	Y.4,166,163.6	Y.4,166,012.2	
Total 3 Lines			865m

[Laboratory test]

	Quantity	Item
Drilled core test	20 Samples	Unconfined compression test etc.
Construction material test	95 Samples (7 sites)	Specific gravity, Soundness etc.





## 7.4 Geology of Reservoir Area

### 7.4.1 Topography

The projected reservoir will have the shape of a bow as a whole with its direction changing from northeast-southwest to north-south to northwest-southeast to east-west in order from the upstreammost part toward the dam. The length will be approximately 11 km with the valley width at high water level (EL. 630 m) approximately 200 m on average.

The mountain masses surrounding the reservoir have elevations from 1,500 to 2,500 m, all of which present rugged mountain forms. The inclinations of the slopes at both banks of the Zamanti River facing the reservoir are steep at approximately 45 deg on average, and at the limestone distribution area at the end of the reservoir the slopes are even steeper to form cliffs of around 70 deg.

The average river-bed gradient of the Zamanti River inside the reservoir is approximately 1/100, and there are no parts of sudden change in the river gradient such as large waterfalls along the way. The principal tributaries merging with the Zamanti River inside the reservoir are the Topaktas River and the Samadan River, both of which join the Zamanti at its right-bank side.

### 7.4.2 Geology

#### (1) Stratification

As shown in Fig. 7-2 and Table 7-4, Mesozoic limestone, melange (complex series), ophiolite, and Quaternary sediments mainly consisting of slope wash and alluvium are distributed in the surroundings of the reservoir.

#### (a) Limestone (Jkr)

Limestone is distributed at the upstreammost part of the reservoir.

The limestone is a gray color, slightly crystalline, and is hard and massive, but bedded limestone of grayish black color can also

be seen at parts. According to the results of chemical analyses of the two, compared with the massive limestone of gray color, the bedded limestone of grayish black is slightly lower in CaO and high in SiO<sub>2</sub> and Al<sub>2</sub>O<sub>3</sub>. The bedded limestone, according to the results of surface geological mapping, is cut by repeated micro-folds, and further, by small faults.

Small faults and joints are developed in the limestone, and especially in the gray, massive limestone, there are thin solutions seen along these fissures.

(b) Complex Series (ks)

Complex series is distributed at the boundary between limestone and ophiolite in the vicinity of the upstreammost part of the reservoir. The thickness is small in comparison with limestone and ophiolite.

Complex series presents various kinds of colors, such as green, red, purple, and brown, and is composed of various kinds of rock blocks. The basement part is generally layered, while the upper part is in the form of irregular blocks. The rocks composing the complex series are fragments (blocks) of ophiolite, chart, limestone, etc.

The areas where complex series is distributed generally are of gentle topography.

(c) Ophiolite (Of)

Ophiolite is widely distributed in the reservoir area except for the upstreammost part of the reservoir.

Ophiolite is a general term for composite rocks made up mainly of ultrabasic to basic rocks such as peridotite, gabbro, diabase, and basalt. The rocks in the reservoir area and in the vicinity of the dam site are of the same qualities when inspected visually, and according to the results of microscopic observations of rock samples collected, all have been found to be peridotite. (Microscopic observation results are given in an appendix.)

Further, since the recent research results (Geologic Map of the KOZAN-J20 Quadrangle, 1987) of MTA GENEL MUDURLUGU also indicate that peridotite is widely distributed in this area, ophiolite will be called peridotite after this in the discussions below.

The peridotite is a compact, hard and massive rock which presents a dark green to grayish black color. The surface of the bedrock is often weathered and discolored to brown, but the depth of weathering is generally shallow. Joints in grid form and small-scale faults without much continuity are developed in the peridotite. Weak serpentinization can be seen along these cracks. A small quantity of chromite is found in the peridotite.

(d) Slope Wash (ym)

Slope wash is deposited in small scale close to the elevation of the river bed at both banks of the Zamanti River. Slope wash deposits in the peridotite distribution zone and in the limestone zone contain boulders of their respective rocks, and generally, there is little fine material.

(e) Alluvium (al)

Alluvium is distributed at the bed of the Zamanti River, and in particular, there are wide distributions at the confluences of the Zamanti River and tributaries. Especially, the confluence of the Topaktas River with the Zamanti has the widest distribution of alluvium within the reservoir area.

The alluvium mainly consists of coarse sand and limestone and peridotite boulders of cobble size, and there is generally little content of fine material.

(f) Top Soil (bt)

Top soil is seen at gently-sloped parts along the Zamanti River. The thickness is thin.

## (2) Structural Geology

### (a) Tectonic Movement

The reservoir area, according to a geological report of the DSI (1988), has been subjected to severe tectonic movements associated with the Hersinian-Alpine orogenic movement.

It is assumed that these severe tectonic movements caused peridotite to ride on top in a manner to push away limestone and the deposits which had been forming overlying the limestone.

### (b) Faults

Boundaries between limestone and peridotite are in the form of thrust faults due to the beforementioned cause. Such thrust faults are distributed in the vicinity of the upstreammost part of the reservoir. Boundaries between limestone and complex series are often in the form of more or less vertical faults, and these faults also are seen in the vicinity of the upstreammost part of the reservoir.

Other than the above, there are numerous smallscale faults that are not continuous for very great lengths seen inside the respective rock facies.

### (c) Joints

Joints are developed inside limestone and peridotite. There are joints in the limestone which are filled with calcite, but openings of several millimeters are seen in most cases. Joints in peridotite are thought to be mainly cooling joints. Open joints are also found at the ground surface, but it is assumed that these are fixed judging by the results of investigations at the dam site described later.

### (d) Landslides and Colluvial Areas

According to aerial-photo interpretation and surface geological mapping results, there are arc-shaped cliffs at places in the complex series and peridotite distribution zones in the surroun-

dings of the reservoir. These arc-shaped cliffs indicate the possibility of collapses or sliding of bedrock at those places, but all are of small scales, and are distributed only at around EL. 1,000 m, considerably above the slopes near the bed of the Zamanti River and the high water level of the reservoir.

#### 7.4.3 Hydrogeology

A spring (Oruc Spring) of flow from 2 m<sup>3</sup>/s to 4 m<sup>3</sup>/s discharged from a cave developed in limestone is seen at the right bank of the Zamanti River at an elevation of 650 m approximately 400 m upstream from the end of the reservoir. There are also numerous caves at around EL. 700 m of the Topaktas River, a tributary of the Zamanti River, and a spring (Kapuz Spring) of around 10 m<sup>3</sup>/s is seen. These springs serve to stabilize the runoff of the Zamanti further downstream.

On the other hand, the peridotite which comprises the greater part of the reservoir does not have any spring locations to speak of in particular. Although there are places at the bottoms of slopes near the river-bed level of the Zamanti where springing occurs, this is water infiltrated from the ground surface that has seeped out through cracks in the bedrock, suggesting that the groundwater tables at both sides of the Zamanti River are high.

In general, gullies in the limestone distribution zone are dry with water flows seen only immediately after rainfall. In contrast, gullies in the peridotite distribution zone have flowing water except during the low-water season.

#### 7.4.4 Considerations from the Viewpoint of Engineering Geology

##### (1) Slope Stability

The area where complex series is distributed is generally of gentle topography, is susceptible to surface erosion, and arc-shaped cliffs are seen. However, the area of complex series distribution itself is small, while the arc-shaped cliffs are distributed in small scale at around EL. 1,000 m, far above the design high water level of the

reservoir, and it is judged they will not harm the stability of the reservoir. The arc-shaped cliffs and slope wash seen in the peridotite distribution zone are of small scale and are not thought will impair the stabilities of reservoir slopes.

(2) Watertightness

Peridotite and complex series which make up the greater part of the reservoir area are impermeable, while the groundwater tables are high and it is thought there will be no problem about watertightness at areas where these rocks are distributed.

On the other hand, based on the contour lines shown on a 1/5,000-scale topographic map, the distribution area of limestone is upstream of EL. 610 m at the bed of the Zamanti River. In effect, in relation to the high water level of the reservoir at elevation of 630 m, a maximum depth of 20 m and a length of approximately 600 m at the end of the reservoir falls into the limestone distribution zone.

The limestone distributed here sandwiches the peridotite distributed widely in the reservoir and at the dam site with the limestone on the downstream side (distributed at the headrace tunnel route), and since the two are of the same quality according to visual inspection, when the circumstance of the peridotite having been thrust on top of the limestone mass by tectonic movement is considered, it cannot be denied that there is a possibility the two limestones are connected together deep underground. Therefore, according to the results of geological and hydrogeological investigations made up to this time, there have been no signs uncovered of water clearly springing from the projected reservoir area, but for the sake of safety, it is suggested there is a necessity for additional investigations to be made to ascertain the watertightness of the upstreammost part of the reservoir.

According to the results of surface geological mapping, there are solution cracks seen along small faults and joints in the limestone distribution zone over a length of 600 m at the upstreammost part of the reservoir. However, large-scale karstic caves are not seen at

least on the slopes of both banks of the Zamanti from the present river bed to EL. 630 m, the high water level.

On the other hand, in the river bed of the Zamanti between EL. 610 to 630 m, there are water springs at places although of small scale. The existence of the springs was ascertained from the fact that in field investigations after rainfall, when the water of the Zamanti River was muddied, springing of clear ground water from the river bed was observed. This indicates that caves in which underground water flows exist in the limestone under the bed of the Zamanti River, and at the same time indicates that such caves do not cause water to leak from the Zamanti River, but conversely function to increase the flow.

From EL. 610 to 630 m at the river bed, there is no part seen that would cause the discharge of the Zamanti River to be suddenly decreased.

As described above, there are no geological or hydrogeological data clearly indicating large amounts of leakage from the limestone distribution zone at the upstreammost part of the reservoir both under present conditions and when the reservoir will have been built.



Table 7-4 Stratigraphic Section of Reservoir Area

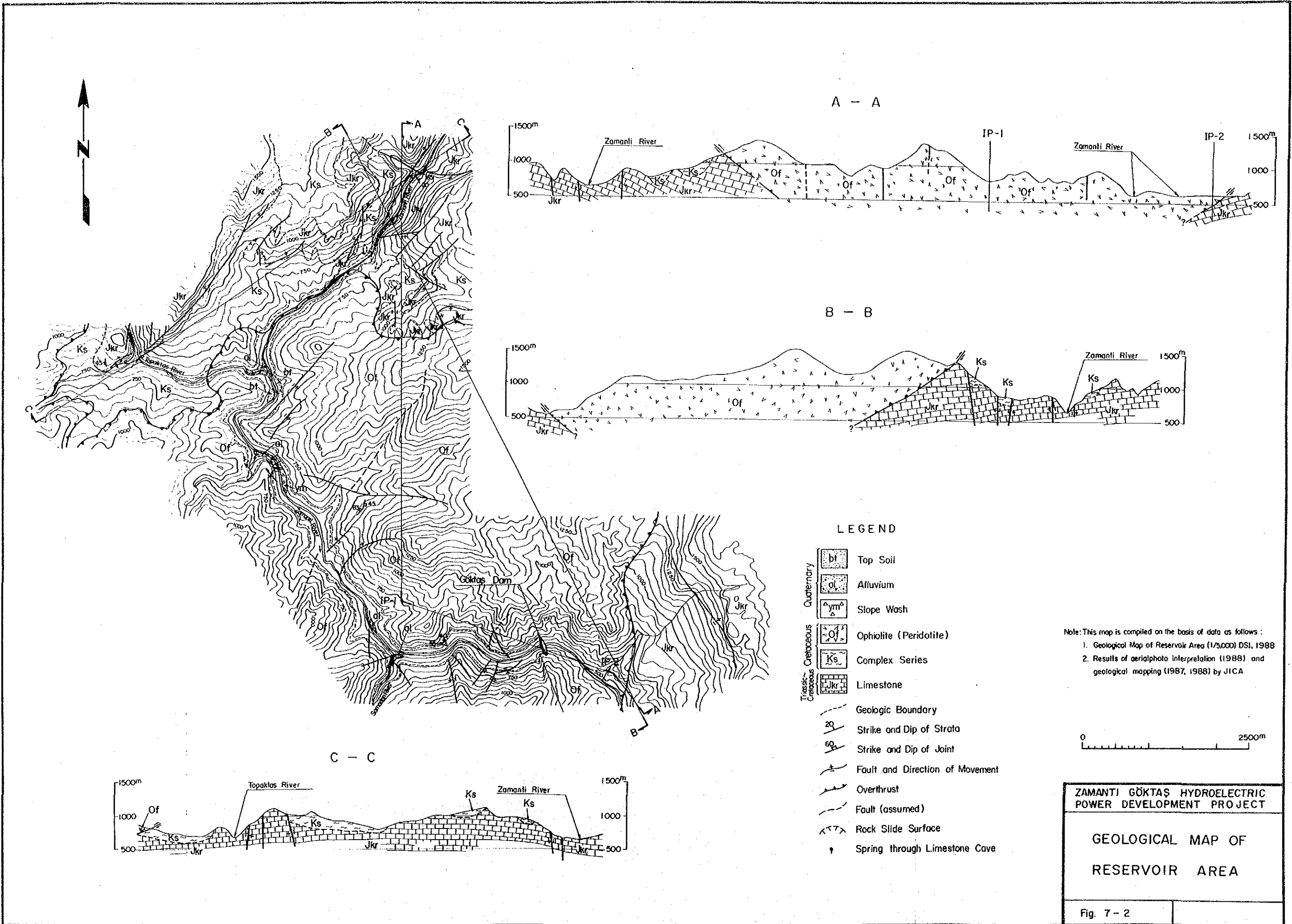
Upper Systems	System	Series	Symbol	Lithology
CENOZOIC	QUATERNARY	HOLOCENE	bt	TOP SOIL As a thin cover.
			ym	SLOPE WASH Gravelly
			al	ALLUVIUM Gravelly
MESOZOIC	JURASSIC ~ CRETACEOUS	UPPER CRETACEOUS	Of	OPHIOLITE Green, brown colored peridotite, dunite. Cracked, fissured at surface.
			Ks	~~~~~ OVER THRUST ~~~~~ COMPLEX SERIES Green ophiolite, serpentinite, radiolarite and limestone, fragmented.
			Jkr	~~~~~ UNCONFORMITY? ~~~~~ LIMESTONE Gray, dark gray colored limestone. Generally massive, bedding in some places. Joints are generally empty. Solusion cracks.

Table 7-5 Chemical Analysis of Limestone in Reservoir Area

Sample No.	Location	Rock Name	(wt.%)						
			SiO <sub>2</sub>	Al <sub>2</sub> O <sub>3</sub>	Fe <sub>2</sub> O <sub>3</sub>	MgO	CaO	SO <sub>3</sub>	
G-3	Outcrop, left bank of Zamanti river at elevation 610 m.	Limestone	0.05	0.02	-	0.16	55.03	0.01	
G-4	Outcrop, right bank of Zamanti river at elevation 630 m.	Limestone (biomicrite)	0.99	2.26	0.34	0.79	51.89	0.19	
G-5	Outcrop, right bank of Zamanti river at elevation 630 m.	Limestone	0.08	0.42	0.15	1.67	53.20	none	









## 7.5. Geology of Dam Site

### 7.5.1 Topography

The dam site is located near EL. 510 m at the bed of the Zamanti River approximately 22 km upstream from the confluence of the Zamanti and the Goksu River, and approximately 21 km north of Karsanti. The Zamanti River which had been meandering from west to east changes its course to the southeast from the vicinity of the dam site.

The slopes at both sides of the dam site comprise steep cliffs close to 90 deg at parts and averaging about 45 deg between a height difference of approximately 500 m from EL. 510 m to EL. 1,000 m. Vegetation is sparse on the whole with much outcropping of basement rock. The slopes at both banks near the dam site have gullies at an average rate of one every 50 m horizontally, which are of small scale but cut deeply into the mountainsides.

The width of the Zamanti River in the vicinity of the dam site is approximately 40 m, the valley width at the design high water level elevation of 630 m being approximately 200 m. The river-bed gradient of the Zamanti in the vicinity of the dam site is approximately 1/80, and there are no parts of sudden changes in the river gradient.

### 7.5.2 Geology

The dam site, as shown in Figs. 7-3 and 7-4, consists of Mesozoic peridotite which is covered at parts by Quaternary sediments such as slope wash and alluvium.

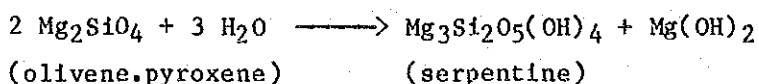
#### (1) Basement Rock

##### (a) Component Rocks

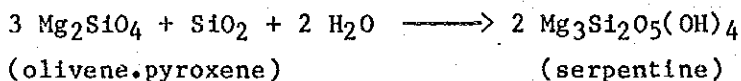
The peridotite which makes up the basement rock for the dam is a compact, hard, and massive rock, dark green to blackish gray in color.

Peridotite may be classified into dunite, wehrlite, harzburgite, and lherzolite depending on the proportions of its rock forming minerals, olivine and pyroxene, and the variety of pyroxene. According to the results of microscopic observations made by the JICA Survey Team, the peridotite at this site may be classified as dunite since most of its rock forming minerals is olivine. (The results of microscopic observations are given in an appendix.)

Peridotite is known to change into serpentine on being subjected to alteration from a reaction with water at comparatively low temperature (under 500°C) called serpentinization. The reaction formula in this case is:



or



The peridotite at this dam site has also been subjected to serpentinization, but the serpentinization is only found thinly along cracks, and is slight as a whole. (The results of X-ray diffraction of serpentine samples collected in the field are given in an appendix.)

(b) Faults

Large-scale faults of great lengths and having wide fractured zones are not distributed in the neighborhood of the dam site. The faults that are recognizable near the dam site are mostly small-scale ones with practically no fillings and weak continuities. Slickensides are seen at the planes of most of these small-scale faults, while in some of the faults, thin vein-like serpentine resulting from serpentinization can be observed. The fault with the most prominent serpentinization is at a point 50 m in horizontal depth in the exploratory adit "DA-1" at the right-bank side of the dam site. This fault has total width of 1 m, and numerous thin veins of serpentine are concentrated in this width.



The strike of this fault is N67°E, 75°NW, roughly parallel to the Zamanti River, but it has not been detected at the ground surface in the vicinity or in drilled holes. Therefore, the continuity of this fault is thought to be no more than 50 m.

At approximately 1.5 km downstream from the dam site, there is a thrust fault in roughly the north-south direction comprising the boundary between the peridotite and limestone on the downstream side. The extreme shearing and alteration due to this thrust fault is not seen in the peridotite distributed at the dam site.

(c) Joints

Joints are developed at intervals of approximately 30 cm on average in the peridotite making up the dam site. Some of these joints are seen to be open near the ground surface, but so far as observed inside exploratory adits they are tightly closed at more than 5 m in horizontal depth. Thin veins of serpentine caused by serpentinization are seen in part of the joints.

(d) Weathering

The surface of the bedrock is weathered and discolored in many cases, but the thicknesses are about several millimeters at maximum. The depths to which weathering and discoloration can be seen along cracks are generally shallow, being from 5 to 10 m from the ground surface.

(2) Surface Deposits

(a) Slope Wash

Slope wash is distributed directly below cliffs at both banks under EL. 550 m. The area of distribution is larger at the left bank compared with the right bank. The slope wash, according to observations at the ground surface is mainly composed of cobble-size and boulder-size angular gravels of peridotite, and the fines content is low. The thickness is estimated to be a maximum of around 10 m at the left bank where the widest distribution is seen.

(b) Alluvium

Alluvial deposits are distributed at the bed of the Zamanti River. The thickness is approximately 23 m at maximum according to the results of drilling at the river bed. The alluvium consists mainly of peridotite gravels of cobble size mixed with small amounts of limestone gravels, and the fines content is low.

(3) Groundwater Table

The water levels in drillholes made at the dam site are as shown in Fig. 7-4. It is estimated from these results that the groundwater table rises from the river bed toward the design high water level along the slopes at both banks.

### 7.5.3 Considerations from the Viewpoint of Engineering Geology

(1) Bedrock Strength

According to the results of laboratory tests on drilled cores conducted by the DSI, the peridotite comprising the dam site has unconfined compressive strengths of 264 kgf/cm<sup>2</sup> to 1,015 kgf/cm<sup>2</sup>, average 576 kgf/cm<sup>2</sup>, and tensile strengths of 63 kgf/cm<sup>2</sup> to 280 kgf/cm<sup>2</sup>, average 125 kgf/cm<sup>2</sup>, as shown in Table 7-6. The test results organized according to the rock evaluations of the sites from which these samples were collected (see "Rock Classifications" of (4) below) are as shown below.

	Rock Evaluation	Test Values (kgf/cm <sup>2</sup> )	Average (kgf/cm <sup>2</sup> )
Unconfined Compressive Strength	(b)	311 - 1,015	625
	(c)	264 - 490	377
Tensile Strength	(b)	63 - 280	122
	(c)	101 - 168	135

Regarding deformation characteristics, according to the results of plate bearing tests inside exploratory adits, modulus of defor-

mation, D, were from 19,200 kgf/cm<sup>2</sup> to 132,100 kgf/cm<sup>2</sup>, average 88,200 kgf/cm<sup>2</sup>, and tangent modulus of elasticity, E, from 57,500 kgf/cm<sup>2</sup> to 239,600 kgf/cm<sup>2</sup>, average 161,700 kgf/cm<sup>2</sup>. Organizing these results according to rock evaluations of the testing locations, the results are as shown in the table below.

	<u>Rock Evaluation</u>	<u>Test Values (kgf/cm<sup>2</sup>)</u>	<u>Average (kgf/cm<sup>2</sup>)</u>
Modulus of Deformation	(b)	107,700 - 132,100	120,000
	(c)	19,200 - 103,100	60,000
Tangent Modulus of Elasticity	(b)	189,200 - 239,600	210,000
	(c)	57,500 - 167,700	120,000

Further, with regard to shear strengths, according to the results of shear tests inside exploratory adits, the estimates obtained were  $C = 50 \text{ kgf/cm}^2$ ,  $\phi = 60 \text{ deg}$  for (b) rock in DA-1 at the right-bank side, and  $C = 40 \text{ kgf/cm}^2$ ,  $\phi = 55 \text{ deg}$  for (c) rock in DA-2 at the left-bank side.

The results of the abovementioned plate bearing tests and shear tests are described in detail in 7.7.

## (2) Discontinuity

With regard to discontinuities existing in the bedrock, there are faults and joints as mentioned previously in 7.5.2. Intercalated materials at these discontinuity planes are generally thin, with the intercalated material often being serpentine in thin veins produced by serpentinization.

The directionality of discontinuities at the dam site indicate the Schmidt's net of Fig. 7-5. This figure was prepared based on the results of measurements on a total of 111 discontinuities observed inside the exploratory adits at both banks. As is clearly shown in this figure, discontinuities in various directions are distributed at this site because of weakness in concentration in a specific direction. A Schmidt's net picking up only discontinuities of thickness 1 mm and over (and generally less than 10 mm) to indicate

their directionalities is shown in Fig. 7-6. From this figure also, it can be comprehended that discontinuities in the east-west direction and the northeast-southwest direction are larger in number, but as a whole, the degree of concentration in a specific direction is not distinct.

The frequencies of discontinuity planes with intercalations of serpentine shown in Fig. 7-6 are roughly the same for the right and left banks, and are one in every 3 to 4 m. (Geological logs of adits and a list of discontinuities are given in an appendix.)

### (3) Permeability

Lugeon tests utilizing drillholes at the dam site were carried out on a total of 7 holes, amounting to 269 stages and a length of 538 m. The Lugeon tests were performed on bedrock excluding the surface deposits with stages at 2-m intervals. The test results are shown in drilling logs in Fig. 7-4.

Lugeon values (Lu) were normally calculated from amounts injected at a pressure of 10 kgf/cm<sup>2</sup>. However, for tests in which injection pressures could not be raised to 10 kgf/cm<sup>2</sup> for some reason, values converted by the following equation were used.

$$\text{Converted Lugeon Value, } Lu' = 10 Q/P \cdot L$$

where, Q: amount injected (ℓ/min)

L: length of section tested (m)

P: injection pressure (kgf/cm<sup>2</sup>)

As shown in Fig. 7-4, values higher than 10 Lu are seen only at surface layer portions of the dam site, and it can be judged that permeability is very low as a whole.

This site is composed of sound peridotite with no water seeping through the rock forming minerals so that permeability depends on cracks, and it is thought that adequate waterstopping treatment can be provided with cement grouting of the kind generally used.

#### (4) Rock Classification

The basement rock of the dam is composed of a uniform peridotite. It may be considered that degree of weathering, hardness, and distribution of discontinuities of bedrock are fundamental factors governing the engineering geological properties of the bedrock.

The bedrock at this site was classified according to the bedrock classification criteria in Table 7-7 based on this thinking. By classifying according to factor in this way, it was though possible for comprehensive rock evaluations to be made. And, it may be understood that by rock evaluation, divisions had been made into grades capable of expressing the engineering geological properties of the rock. The combinations of bedrock classification factors and criteria for comprehensive rock evaluations (consisting of 5 grades from (a) to (e)) are shown in Fig. 7-7.

According to the results of investigations of all exploratory adits and drilled cores of the dam site and its neighborhood, the peridotite comprising the dam site was found to be 2 B III in the classification, that is, bedrock which is fresh and hard, with crack spacing from 20 cm to 40 cm predominant. In rock evaluation, the grade is (b).

Although there is distribution also of Grade (c) rock, this dam site with Grade (b) most predominant is judged to possess ample suitability for construction of a concrete dam of 150-m class height in view of the previously-described mechanical and hydrogeological properties.

#### (5) Selection of Dam Axis

Regarding the dam axis in the Goktas Project, as shown in Fig. 7-8, two dam axes, Dam Axis I and at a point approximately 1.3 km upstream, Dam Axis II, were selected at the Master Plan stage, while later, Dam Axis A (downstream side) and Dam Axis B (upstream side) were selected between the first two by the DSI.

The JICA Survey Team carried out surface explorations based on 1/5,000 and 1/1,000 topographical maps, and aerial-photo interpreta-

tions on these selected dam axes. As a result, the vicinity of Dam Axis A (slightly upstream of Dam Axis A) was selected based on the following reasons:

- o Parts of bedrock that have been altered are found at the left-bank sides of the upstream Dam Axis II and Dam Axis B.
- o Gullies cutting deep into the mountainsides exist in the vicinity of Dam Axis B.
- o The valley width in the vicinity of the downstream Dam Axis I is large compared with the other dam axes, while moreover, altered parts of bedrock can be seen.
- o The vicinity of Dam Axis A has less bedrock that has been altered compared with other dam axis sites.
- o The vicinity of Dam Axis A can be judged to possess ample suitability as a dam site according to various geological investigations as stated up to the preceding clause.

(6) Dam Type

This site does not involve any problem regarding mechanical and hydrogeological properties as the foundation rock for a rockfill dam, but suitable core material is not distributed in the vicinity of the dam site, while the valley width is narrow and it is topographically difficult for a spillway to be provided. Therefore, it is thought adopting a rockfill type for this site will not be very advantageous.

In case of considering a concrete type dam, it is judged there will be no mechanical or hydrogeological problem. Further, in the event a thin arch dam is selected, it is thought necessary for thorough studies to be made on giving consideration to the facts that serpentinization although slight can be recognized and that the topography is extremely complex.

Table 7-6 Laboratory Test Results of Drilled Cores at Dam Site

Drillhole No.	Depth (m)	Rock Name	* (1) Specific Gravity	* (1) Absorption (%)	* (2) Unconfined Compression Strength (kgf/cm <sup>2</sup> )	* (3) Tensile Strength (kgf/cm <sup>2</sup> )
SK-3	33.6 - 34.0	Peridotite	3.15	0.2	948.1	82.3
SK-3	88.6 - 89.1	"	3.31	0.3	730.9	139.9
SK-4	16.0 - 16.3	"	3.27	0.1	365.6	62.9
SK-4	51.7 - 52.0	"	3.10	0.6	311.1	70.0
SK-4	75.5 - 76.0	"	3.24	0.2	264.4	101.2
SK-5	61.2 - 61.4	"	3.29	0.2	489.7	168.0
SK-5	76.0 - 76.4	"	3.22	0.2	629.6	139.9
SK-5	95.6 - 96.0	"	3.30	0.1	454.9	62.9
SK-6	36.0 - 36.5	"	3.30	0.1	548.4	138.2
SK-6	89.4 - 89.8	"	3.31	0.1	1,014.5	279.8

Note: \*(1) ASTM C97-83  
 \*(2) ASTM D2938-79  
 \*(3) ASTM D3967-81

Table 7-7 Standard of Rock Classification

for Adit

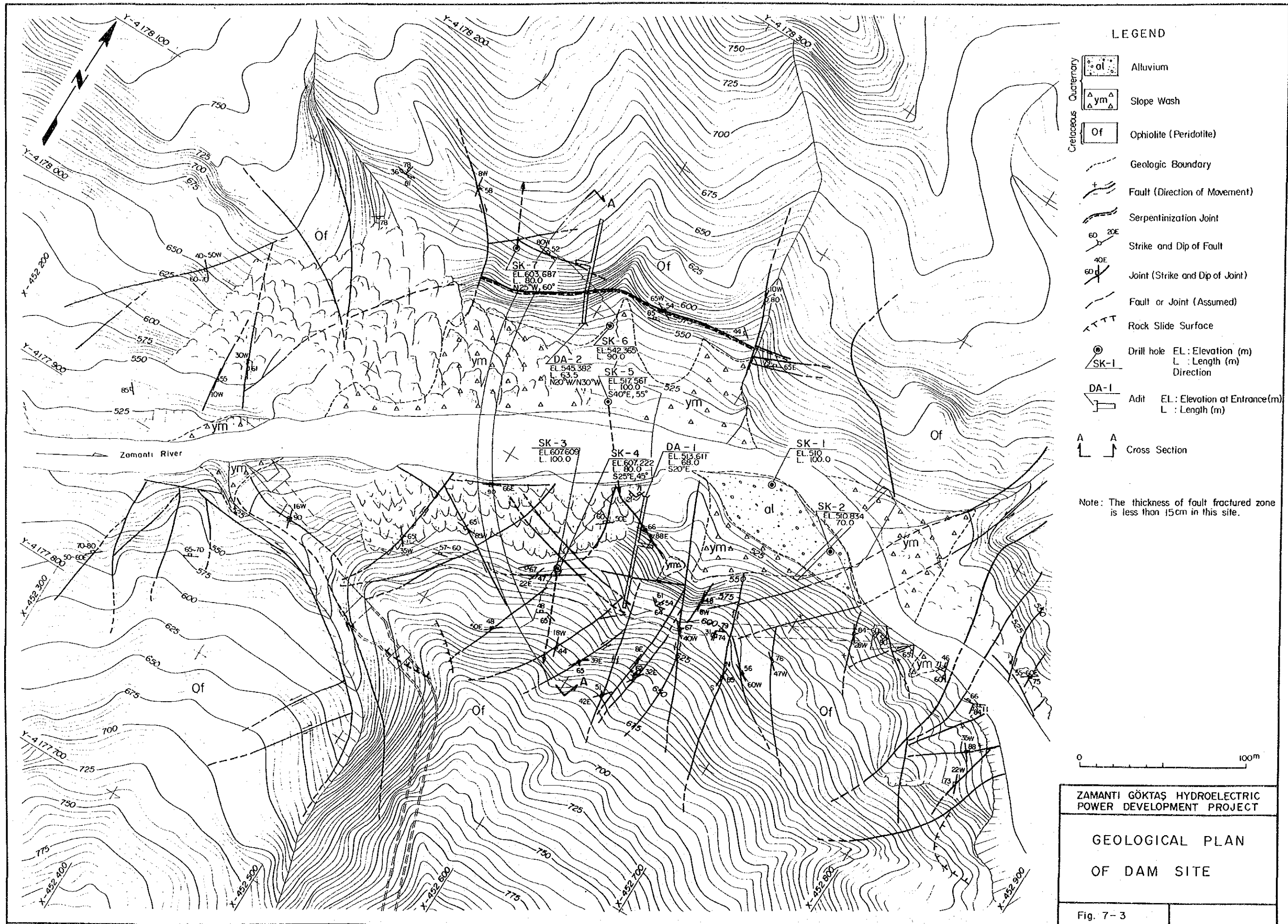
Weathering		Hardness		Interval of Cracks	
1	Very fresh. No weathering of mineral component.	A	Very hard. Broken into knifedged pieces by strong hammer blow.	I	Over 100 cm
2	Fresh. Some minerals are weathered slightly. Usually no brown crack.	B	Hard. Broken into pieces by strong hammer blow.	II	40 - 100 cm
3	Fairly fresh. Some minerals are weathered. Cracks are stained and with weathered material.	C	Brittle. Broken into pieces by medium hammer blow.	III	20 - 40 cm
4	Weathered. Fresh portions still remain partially.	D	Very brittle. Easy broken into pieces by medium hammer blow.	IV	5 - 20 cm
5	Strongly weathered. Most minerals are weathered and altered to second minerals.	E	Soft. Able to dig with hammer.	V	Under 5 cm

for Drilled Core

Weathering		Hardness		Interval of Cracks	
1	Very fresh. No weathering of mineral component.	1	Very hard. Broken into knifedged pieces by strong hammer blow.	1	Over 30 cm
2	Fresh. Some minerals are weathered slightly. Usually no brown crack.	2	Hard. Broken into pieces by strong hammer blow.	2	10 - 30 cm
3	Fairly fresh. Some minerals are weathered. Cracks are stained and with weathered material.	3	Brittle. Broken into pieces by medium hammer blow.	3	3 - 10 cm
4	Weathered. Fresh portions still remain partially.	4	Very brittle. Easy broken into pieces by medium hammer blow.	4	1 - 3 cm
5	Strongly weathered. Most minerals are weathered and altered to second minerals.	5	Soft. Able to dig with hammer.	5	Under 1 cm







LEGEND

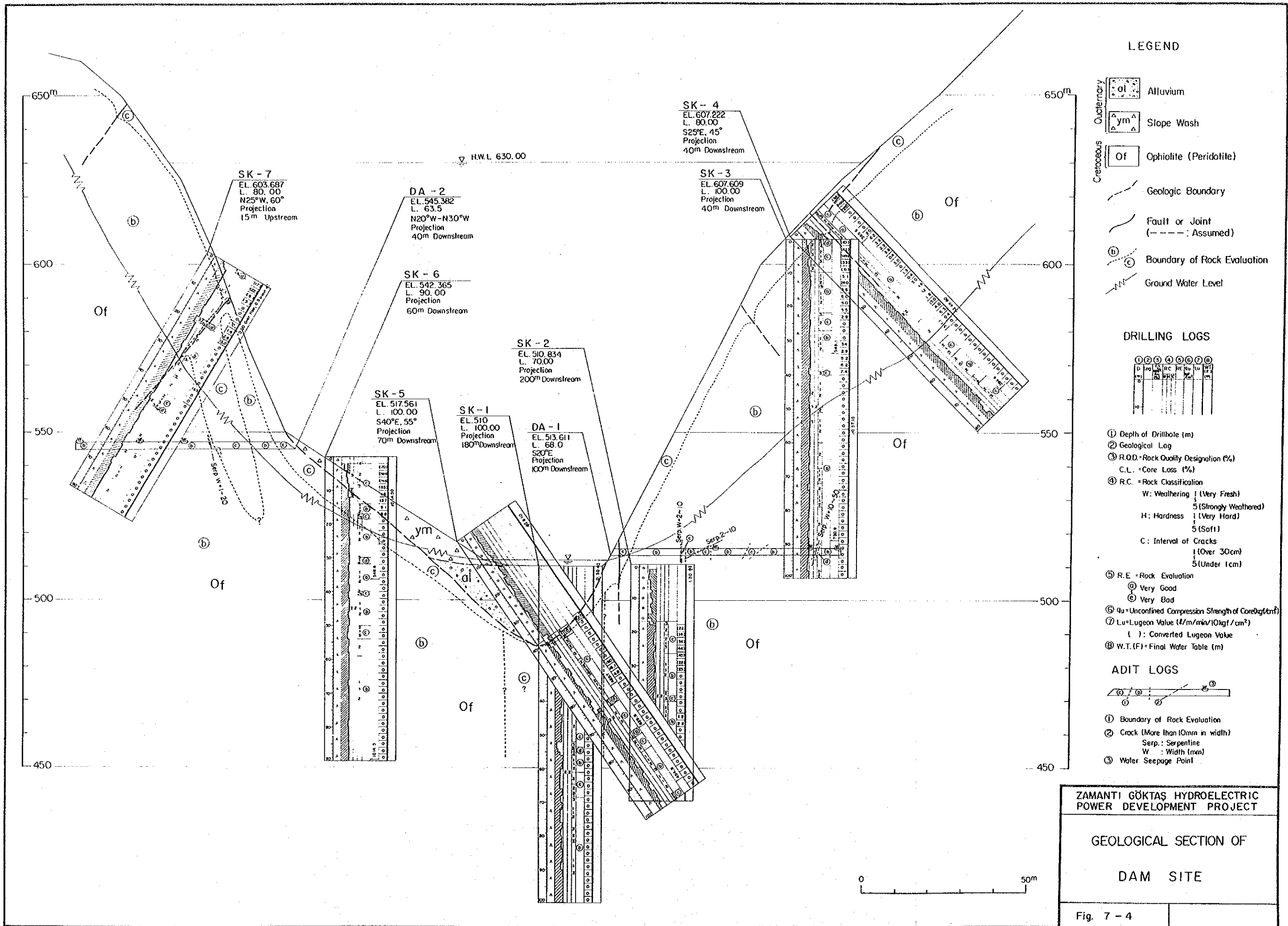
- Quaternary
  - al Alluvium
  - ym Slope Wash
- Cretaceous
  - Of Ophiolite (Peridotite)
- Geologic Boundary
- Fault (Direction of Movement)
- Serpentinization Joint
- Strike and Dip of Fault
- Joint (Strike and Dip of Joint)
- Fault or Joint (Assumed)
- Rock Slide Surface
- Drill hole EL: Elevation (m)  
L: Length (m)  
Direction
- Adit EL: Elevation at Entrance (m)  
L: Length (m)
- Cross Section

Note: The thickness of fault fractured zone is less than 15cm in this site.

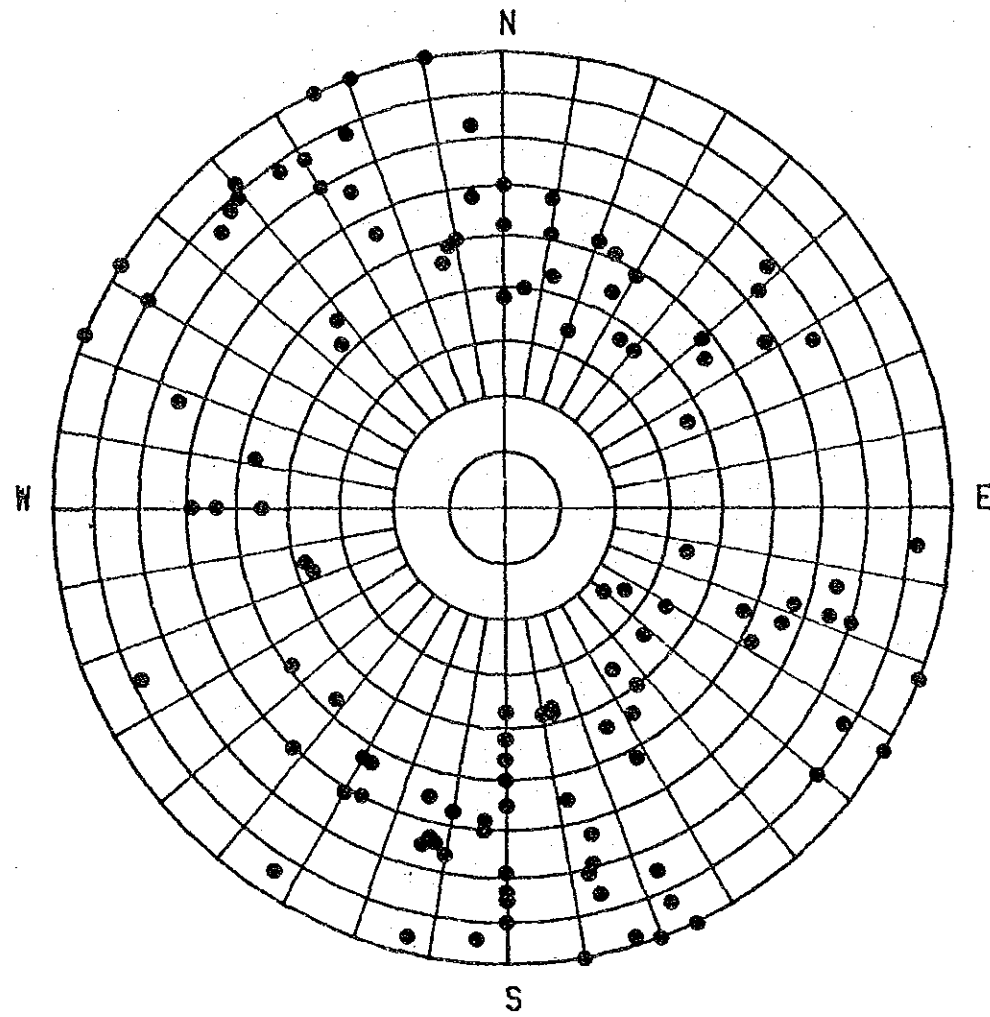
0 100m

ZAMANTI GÖKTAŞ HYDROELECTRIC POWER DEVELOPMENT PROJECT	
GEOLOGICAL PLAN OF DAM SITE	
Fig. 7-3	





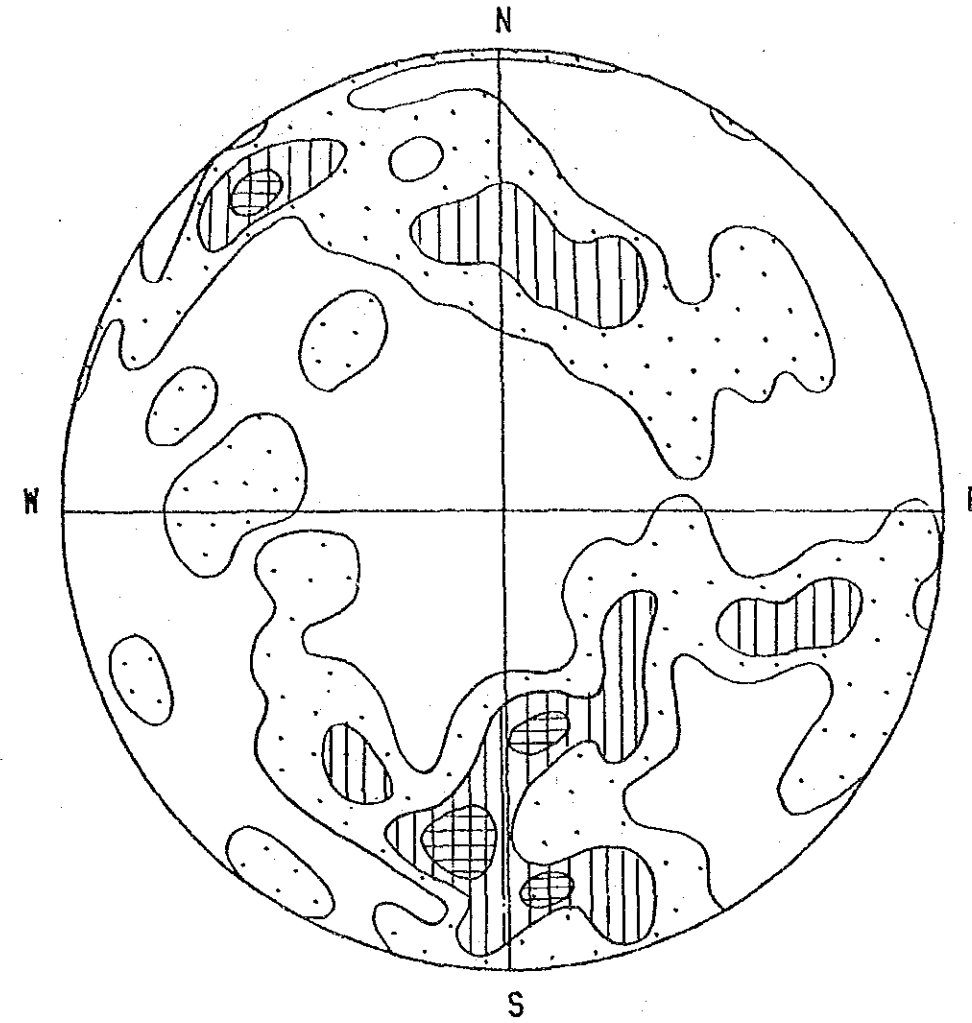




Point Diagram

Schmidt's Polar Net  
Lower Hemisphere Projection

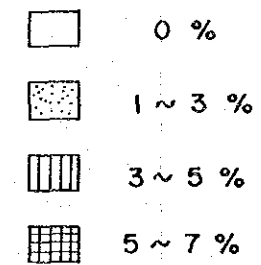
Number of Sample : 111



Contour Diagram

Schmidt's Polar Net  
Lower Hemisphere Projection

Concentration Percentages

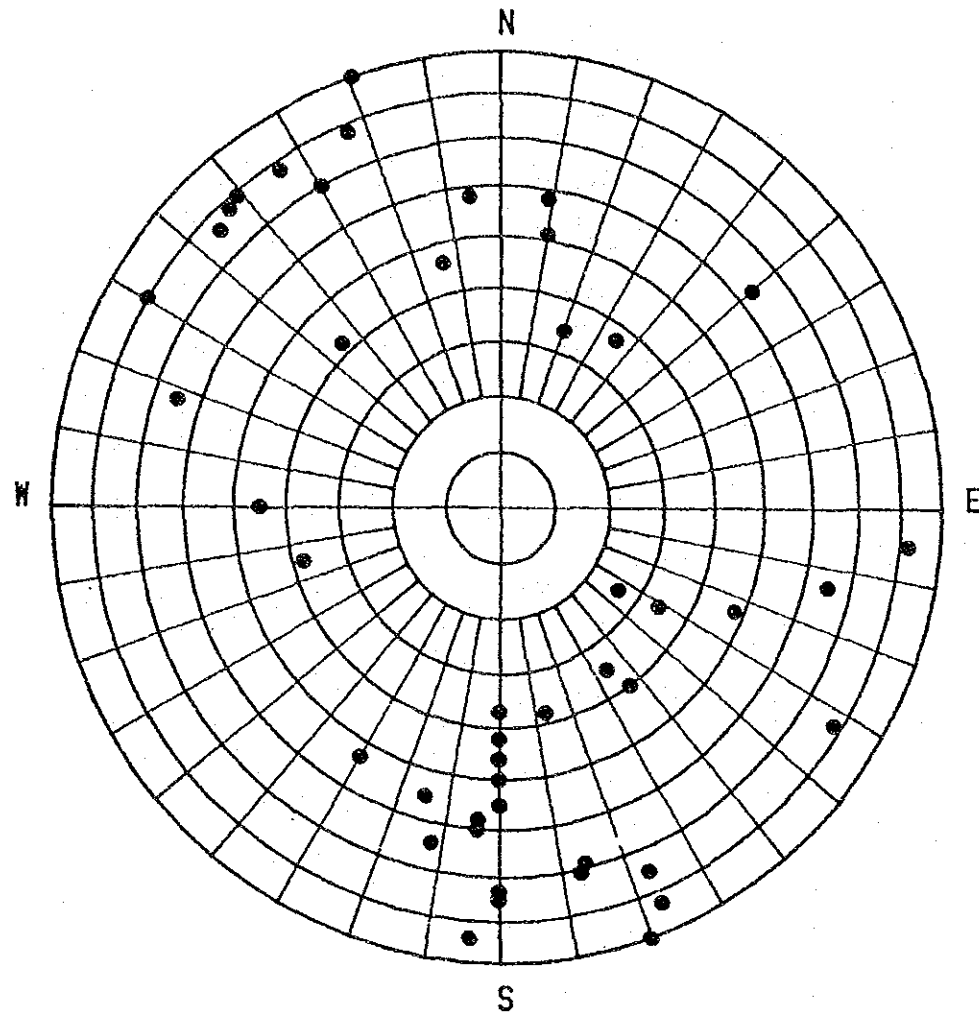


ZAMANTI GÖKTAŞ HYDROELECTRIC  
POWER DEVELOPMENT PROJECT

POINT AND CONTOUR  
DIAGRAMS OF ALL MEASURED  
CRACKS IN ADITS

Fig. 7-5

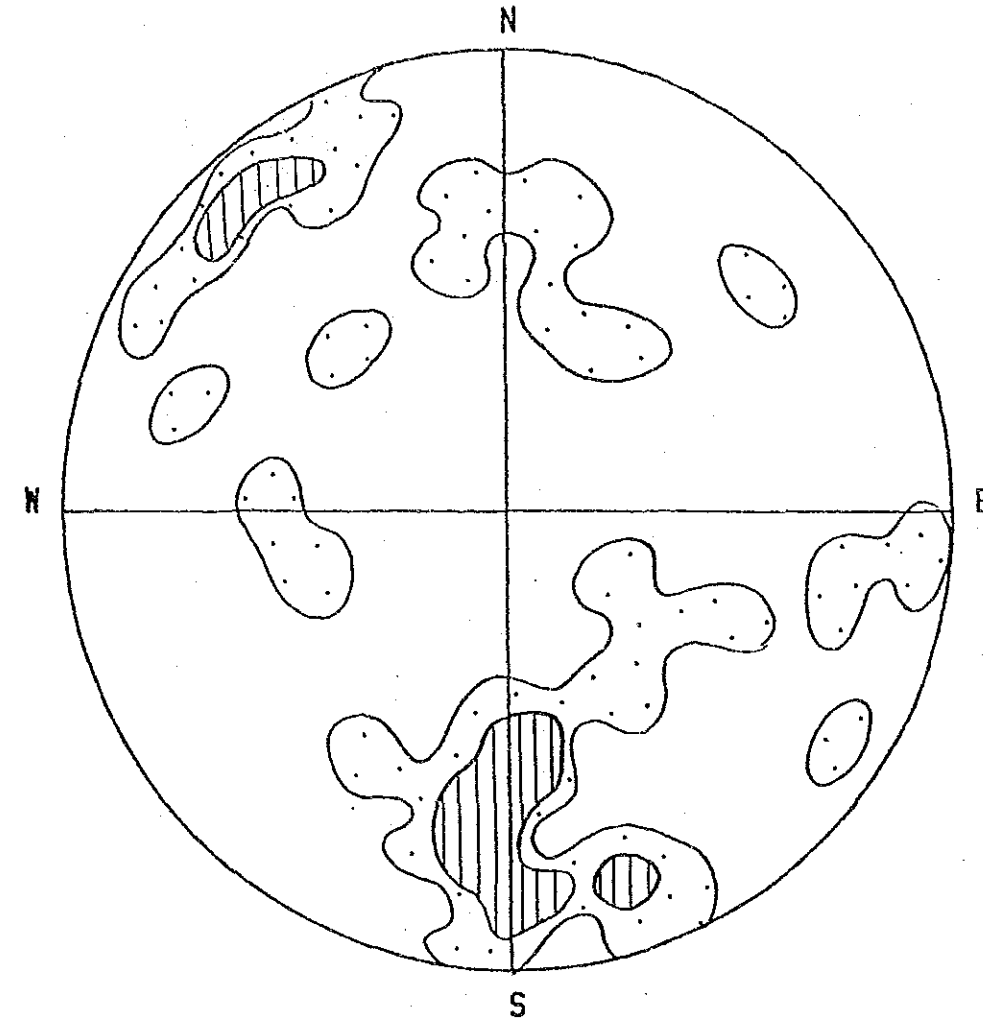




Point Diagram

Schmidt's Polar Net  
Lower Hemisphere Projection




Number of Sample : 45



Contour Diagram

Schmidt's Polar Net  
Lower Hemisphere Projection

Concentration Percentages

-  0 %
-  2 ~ 5 %
-  5 ~ 10 %

ZAMANTI GÖKTAŞ HYDROELECTRIC  
POWER DEVELOPMENT PROJECT

POINT AND CONTOUR  
DIAGRAMS OF SERPENTINIZATION  
CRACKS IN ADITS

Fig. 7-6





Fig. 7-7 ROCK EVALUATION

		Hardness <sup>*(1)</sup>				
		A	B	C	D	E
Interval of Cracks <sup>*(1)</sup>	I	(a)	(a)	*(2)	*(2)	*(2)
	II	(a)	(a)	*(2)	*(2)	*(2)
	III	(b)	(b)	(c)	*(2)	*(2)
	IV	(c)	(c)	(d)	(e)	*(2)
	V	*(2)	(d)	(d)	(e)	(e)

Notes: \*(1) See Table 7-7 "Standard of Rock Classification".  
 "Weathering" grade is "2"  
 In case of the low grade "Weathering", shift  
 to the low grade "Rock Evaluation".

\*(2) Rare cases.





